m6a methylation orchestrates IMP1 regulation of microtubules during human neuronal differentiation

Authors: Pierre Klein[1,2], Jasmine Harley[2,3], Harry Crook[1,2], Sofia Esteban Serna[1], Theodoros I. Roumeliotis[4], Jyoti S. Choudhary[4], Anob M Chakrabarti[2], Raphaëlle Luisier[5], Rickie Patani[2,3]*, Andres Ramos[1]*

Affiliations

[1]Division of Biosciences, Institute of Structural and Molecular Biology University College London, Darwin Building, Gower Street, London, WC1E 6XA, UK
[2]The Francis Crick Institute, 1 Midland Road, London NW1 1AT, UK
[3]Department of Neuromuscular Diseases, Queen Square Institute of Neurology, University College London, London WC1N 3BG, UK
[4]Functional Proteomics team, The Institute of Cancer Research, 237 Fulham Road, London SW3 6JB, UK
[5]Genomics and Health Informatics Group, Idiap Research Institute, Centre du Parc, 19 rue Marconi, 1920, Martigny, Switzerland

Correspondence to a.ramos@ucl.ac.uk and rickie.patani@ucl.ac.uk

Abstract

Human neurodevelopment requires differentiating neurons to establish large networks of connections in a highly stereotyped manner. Neuronal differentiation in particular requires RNA-binding proteins to spatiotemporally regulate thousands of different mRNAs. Yet how these proteins precisely relate to neuronal development and coordinate the expression of functionally coherent genes in a cell-type specific manner is only partially understood.

To address this, we sought to establish how the paradigmatic RNA-binding protein IMP1/IGF2BP1, an essential developmental factor, selects and regulates its RNA targets transcriptome-wide during the differentiation of human neurons.

We used a combination of system-wide and targeted molecular analyses to show that IMP1 directly binds to and regulates the expression of a large set of mRNAs that govern microtubule assembly, an essential process and a key driver of neuronal differentiation. We also show that m6A methylation during the transition from neural precursors to neurons drives both the selection of IMP1 mRNA targets and their protein expression. Our findings establish m6A methylation as a key mechanism coordinating the regulatory action of IMP1 on human neuronal architecture.

Introduction

During development, neurons establish inter-cellular networks that acquire, retain and respond to information in a spatiotemporally regulated manner. The architectural development of neurites and synapses, and the underlying cytoskeletal changes, require the regulation of gene expression programs by neuronal RNA-binding proteins (RBPs). While the action of these proteins on individual targets has been studied in detail, our understanding of how RBPs regulate networks of genes and orchestrate cellular processes during neuronal differentiation remains limited.

IMP1 is a well-studied RBP that is essential for embryonic development [1,2]. In developing neurons, IMP1 plays a key role in establishing neurite outgrowth and synaptogenesis [3–5]. At the molecular level, IMP1 regulates distinct post-transcriptional steps, including mRNA localisation, stability and translation [6–11]. Molecular studies have focused on the physical and functional interactions with a small number of mRNA targets. In particular, the interaction between IMP1 and beta-actin mRNA has been used as a model system to specifically explore the concept of an RNA 'zipcode' in the regulation of mRNA transport and translation in the cell [7,12,13]. However, how IMP1 may regulate global gene networks underlying the establishment of neuronal architecture remains unclear and is an important open question in neuronal development.

Here, we examine the global role of IMP1 during the differentiation of human neurons to elucidate how this paradigmatic protein is regulated by developmental context and how it controls the expression of essential gene programs. We show that IMP1 RNA target selection is regulated by an increase of m6A methylation during the transition from neural precursor cells (NPCs) to neurons, and establish IMP1 as an important regulator of the microtubule network during neuronal development.

Main text

IMP1 regulates microtubule assembly during human neurodevelopment

RNA binding proteins have been shown to perform cell-type specific functions, with key functional determinants considered to be the mRNAs to which the protein is bound and the specific sites the protein interacts with. IMP1 plays an important role in a range of processes essential to the development of the nervous system, including synaptogenesis, dendritic arborisation and axonal pathfinding, among others [4,14]. In order to identify the molecular phenomena underlying these processes, we have used a human induced pluripotent stem cell (hiPSC) differentiation model, and interrogated the developmental transition from NPCs to (isogenic) neurons. In this process, differentiating NPCs undergo major morphological changes to become neurons by building a network of neurites and forming synapses (**Fig. 1a, Extended Data Fig. 1a**). We confirmed the expression of IMP1 in these two stages of development and its distribution in developing neurites (**Fig. 1b,c, Extended Data Fig. 1b,c,d**). Then, we probed protein function by examining two important neuronal differentiation processes which have previously been associated with IMP1: synaptic development and neurite branching [3,4]. Using the pre- and post-synaptic markers SYT-1 and Homer-1, we showed that IMP1 is present in synapses (**Fig. 1c)** and that IMP1 knockdown (KD) downregulates the size (but not the number) of SYT-1 positive synaptic puncta (**Fig.**

1c,,Extended Data Fig. 1e). Furthermore, a morphological analysis of neurite branching revealed a significant decrease in complexity in IMP1 KD neurons compared with their control counterparts (**Fig. 1d**). Together, these data show that IMP1 regulates multiple global cellular processes in differentiating neurons.

In order to investigate the role of IMP1 during neuronal development, we used quantitative mass spectrometry to profile the proteome of NPCs and neurons, in control and IMP1 knockdown conditions. In NPCs, a similar number of proteins are up and downregulated upon IMP1 KD, while in neurons twice as many proteins are downregulated upon KD compared to upregulated (**Fig. 1e,f, Extended Data Fig. 1g**). IMP1 regulation was validated, in a representative subset of targets in neurons using western blot (WB) (**Extended Data Fig. 1f**), confirming that IMP1 modulates protein abundance in a developmentally controlled manner (**Fig. 1e, f, Extended Data Fig. 1g)**. A global functional analysis of the regulated targets indicated that IMP1 regulation of neuronal specialization is organised in gene networks underlying important cellular processes with two of the most highly represented categories of IMP1-regulated targets being related to synapses and microtubule regulation (**Fig. 1g**). The latter includes tubulins, and regulators of microtubule stability such as kinases and microtubule-binding proteins. This suggests that IMP1 plays a coordinated role at multiple levels of microtubule regulation (**Fig. 1g**). An unbiased analysis of the relationship between IMP1-regulated proteins revealed that they interact both physically and functionally, creating a connected network (**Fig. 1h**). This global and quantitative analysis of IMP1 regulation in neurons indicates that, in addition to interacting with kinesins moving on the microtubule transport system to organise local mRNA translation, as previously reported [6,12,15], IMP1 also regulates the microtubule network itself.

Notably, analysis of RNAseq data from NPCs and neurons in both control and IMP1 KD conditions showed that IMP1-mediated regulation of the microtubule gene network does not occur at the mRNA level but rather at the protein level. This is evidenced by discordant changes in IMP1 protein and RNA targets upon KD, with most proteins being downregulated in neurons while this is not the case for the corresponding mRNAs (**Extended Data Fig. 1h**). The regulation mode we observe is therefore different from the RNA stabilisation function of IMP1 reported in cancer cells and other cell lines [8,9,16,17]. It also does not appear comparable to the well-studied regulation of beta-actin local translation [4,18,19] as this protein was not significantly dysregulated following IMP1 knockdown (**Extended Data Fig. 1f**). At the molecular level, this seems more akin to a recently proposed translational regulation of IMP1 in cancer cells models, although the underlying mechanism and full scope have yet to be defined [9,20].

A developmental change in IMP1 protein-RNA interactome underlies microtubule regulation

Next, we wanted to define the dynamic modulation of the IMP1 protein-RNA interactome during neuronal differentiation and, importantly, to establish whether IMP1-mediated regulation of the proteome is directly linked to its interaction with target mRNAs. To this end, we performed IMP1 individual-nucleotide resolution UV crosslinking and immunoprecipitation (iCLIP) on NPCs and neurons **(Fig. 2a,b, Extended Data Fig. 2a,b,c)** yielding an average of 3 million unique reads in NPC and 4 million in neurons. IMP1 crosslink sites were predominantly located in 3'UTRs, similar to what has been previously reported in CLIP studies of highly-proliferative and cancer cells [9,17]. Importantly, comparison of binding in the

two cell types revealed that the IMP1-binding landscape is developmentally regulated, with an increase from 45% to 70% of 3'UTR binding during the transition from NPCs to neurons **(Fig. 2c**). Further, the analysis of the mRNAs interacting with IMP1 indicated that the protein binds to a large set of targets in NPCs and neurons, but with a substantial proportion being developmental stage-specific (**Fig. 2d, Extended Data Fig. 2d**). A Gene Ontology analysis of specific IMP1 targets at the two developmental stages identified pathways related to early neuronal differentiation processes such as spinal cord patterning, chromatin reorganisation and synaptic development in the NPCs, while in neurons revealed pathways related to later stages of neuronal development such as axonogenesis, synapse maturation and microtubule polymerisation (**Fig. 2e and Extended Data Fig. 2e)**. These terms are consistent with the morphological changes we observe during neuronal differentiation upon IMP1 KD (**Fig. 1c, d**). Finally, changes in IMP1-RNA binding during differentiation can be visualised directly by examining iCLIP tracks of individual mRNAs, that show changes between NPCs and neurons both in upregulated genes and in genes with stable expression (**Fig. 2f**).

We then re-examined the IMP1-regulated proteome in NPCs and neurons considering only targets that were directly bound by the protein using our iCLIP assays. We found a striking enrichment in the proportion of downregulated targets upon IMP1 KD in neurons . – there is a 5-fold difference between down and upregulated proteins in the IMP1-bound targets (**Fig. 3a**). Interestingly, in NPCs we also observed a modest 2-fold increase in the downregulated compared with upregulated targets upon IMP1 KD (**Fig. 3a, Extended Data Fig. 3b**). Beyond linking protein regulation to IMP1 binding, the changes in downregulated targets also indicate that a functional specialisation of IMP1 takes place during neuronal development. We validated these findings using siRNA knockdown and quantitative immunocytochemistry (**Fig. 3b, Extended Data Fig. 3a)**, as an orthogonal experimental approach.

A more in-depth analysis of the IMP1 binding pattern showed that targets positively regulated by the protein have a significantly higher number of binding sites compared to unchanged or negatively regulated targets (**Extended Data Fig. 3c**). Notably, this regulation is again found on microtubule-related targets (**Fig.3c),** and directly linked to the number of IMP1 peaks in a transcript (**Fig. 3d)**. These two observations indicate that the regulation of protein abundance observed during neuronal development is linked to the direct binding of IMP1 protein. Importantly, the enrichment in IMP1 binding within the regulated targets is specific to microtubules and neuronal processes (**Fig. 3e)**. This indicates that the regulation of microtubule assembly is a key function of IMP1 in developing neurons. Importantly, it also confirms that IMP1's function in neuronal development is mediated by the regulation of a large gene network, as visualised by the relations between the IMP1-regulated microtubule factors (**Fig. 3f**).

We wondered whether the increase in the number of IMP1 peaks in microtubule-related targets in neurons, and the regulation discussed above, could be explained by an increase in protein or RNA concentration. However, IMP1 concentration decreases during the transition from NPCs to neurons **(Extended Data Fig. 1b**). In addition, while an increase in mRNA concentration can explain increased protein occupancy in some targets, we also observe the presence of new crosslink sites in transcripts with a stable level of expression during development (**Fig. 2f**). This implicates a regulatory mechanism that favours binding to newly expressed neuronal targets.

RNA methylation regulates IMP1-mediated effects on microtubule assembly

The comparison of the IMP1 binding pattern within individual genes with similar expression at different stages of development indicates that the iCLIP peaks of a gene in NPCs and neurons can change independently of its expression level (**Fig. 2f)**. Therefore, this implies an additional regulatory layer in IMP1 RNA target selection. Notably, the neuronal transcriptome has been reported to be highly enriched in m6A methylation [21–25]. In addition, IMP1 binding to m6A has been recently reported to regulate c-Myc and cell cycle targets in cancer cells [9] - and our unpublished biophysical data (Nicastro, Abis et al, under consideration) shows that IMP1 directly recognises m6A in a range of sequences with in-built specificity. To determine whether IMP1 regulation of the microtubule network during neuronal development is mediated by m6A methylation, we characterised the relationship between m6A methylation and RNA binding during the NPC-to-neuron transition. While a number of recent studies have mapped m6A methylation to the transcriptome of human and mouse neurons, m6A methylation of the human transcriptome during neuronal differentiation has remained elusive. To directly compare the IMP1 RNA-binding peaks obtained from our iCLIP assays to neuronal m6A sites, we performed miCLIP assays on the aforementioned human NPCs and isogenic neurons (**Fig. 4a,b)**. The miCLIP dataset included an average of 1 million unique reads for NPCs and 4 million for neurons with high reproducibility of sites between replicates in both cell types (**Extended Data Fig. 4a,b**). As expected, the crosslink sites were enriched in the evolutionarily conserved DRACH consensus motif (D = A/G/U, R = A/G, H = U/A/C) and preferentially localised around the stop codon [21,22] (**Fig. 4c, Extended Data Fig. 4c)**

Interestingly, starting from a similar quantity of RNA, we detected a 5-fold increase in the number of m6A sites in neurons compared to NPCs (**Fig. 4d)**. A molecular rationale for this change is provided by the concurrent increase we observed in the level of the m6A methyl-transferase METTL3 together with the decrease in the level of the ALKBH5 demethylase (**Extended Data Fig. 4d**). Importantly we found the presence of both common and specific m6A sites in the two cell types, indicating a regulated role of methylation during neuronal differentiation (**Extended Data Fig. 4e**). Comparing our data to 6 RNA methylation datasets from neural tissue spanning 3 species showed a substantial overlap in m6A sites (21%) (**Extended Data Fig. 4f**). We then intersected our proteomics, iCLIP and miCLIP datasets and examined how RNA methylation relates to i) IMP1 protein-RNA binding, ii) IMP1 regulation of protein abundance. This revealed that, in neuron-specific targets, the mRNAs encoding proteins downregulated in the IMP1 KD experiment have a higher number of IMP1-m6A peaks compared to proteins that are not regulated (**Fig. 4e**). This overall increase in IMP1 target expression is directly correlated to the number of m6A-IMP1 sites (**Fig. 4f**). We then linked this increase to functional enrichment of IMP1 regulation, and quantified the number of IMP1-m6A sites for different GO categories. As expected, targets related to microtubule regulation and neuronal pathways show a significantly higher number of m6A-IMP1 sites compared to unrelated pathways (**Fig. 4g**). Consistent with the role that methylation plays in IMP1-mediated regulation of the microtubule network, the proportion of the IMP1-upregulated proteins that are part of the microtubule network increases as we filter our MS data for i) IMP1-bound targets and ii) IMP1-m6A bound targets (**Fig. 4i**). To confirm the observed regulatory effect of IMP1 binding to m6A we used siRNA to transiently knock-down the m6A methyltransferase METTL3 in neurons (**Fig. 4h**). We deliberately designed a partial KD, noting that more substantial METTL3 KD has been linked to cell death [26,27].

Reducing the level of METTL3 resulted in a decrease of three representative targets, the microtubule protein TUBB4A and the regulators DCX and MAP2 (**Fig. 4h)**, thus confirming the role of m6A in the regulation of a network of microtubule protein expression.

Discussion

Neuronal differentiation is coupled to an upregulation of microtubule factors that allow the assembly of cytoskeletal structures underlying the development of neurites and synapses [28–30]. An important question in neuronal development is how RNA-binding proteins can control this complex process. Here we show that IMP1, an essential factor for neuronal differentiation, binds and regulates a large and diverse network of tubulins and regulatory factors during the transition between neuronal precursors and differentiated neurons.

The understanding of how IMP1 and similar proteins coordinate morphological changes in developing neurons requires consideration of the system-wide regulatory action of these proteins, which is well-studied in highly proliferating cells but not so in neurons. In particular, a key aspect of global protein function is the selection of the RNA targets. Our iCLIP data indicate, in addition to an increase in the concentration of neuronal RNAs, a specialisation of IMP1 to neuronal targets. Notably, we show that IMP1 binding and regulation of the mRNA targets is not accompanied by the upregulation of the IMP1 protein itself but rather a decrease in the concentration of IMP1.

Importantly, our data show a substantial increase in the transcriptome's m6A 'blueprint' during the NPC-to-neuron transition in human neurodevelopment, likely mediated by the upregulation of the METTL3 m6A writer enzyme and downregulation of the ALKBH5 eraser enzyme. This change in methylation increases the number of IMP1 binding peaks in neuronal RNAs, indicating a higher occupancy of the regulated transcripts. Indeed, IMP1-regulated protein expression of microtubule network targets is m6A dependent. This suggests a mechanism where a lower protein concentration and a site-specific increase in affinity mediated by m6A methylation together increase IMP1 selection of neuronal (microtubule) targets (**Fig. 4j**). The protein interaction with individual RNAs likely depends on the availability of protein and the affinity of individual binding sites. In conditions of limited protein availability, methylation further enhances the capacity of the highly expressed neuronal target mRNAs to functionally interact with the protein.

This model proposes that during neuronal differentiation, distinct regulatory layers converge with an increase in the concentration of neuron-specific targets to mediate functionally viable interactions and promote the required morphological changes. Neuronal mRNAs have been reported to be highly enriched in m6A, and several non-canonical m6A readers (e.g. FMRP, hnRNPA2B1) have been reported to play a role in neuronal differentiation. The developmentally-regulated molecular mechanism of IMP1 specialisation that we describe here likely represents a more widely applicable design principle in the regulation of morphological changes that accompany cell state transitions during development.

Figures

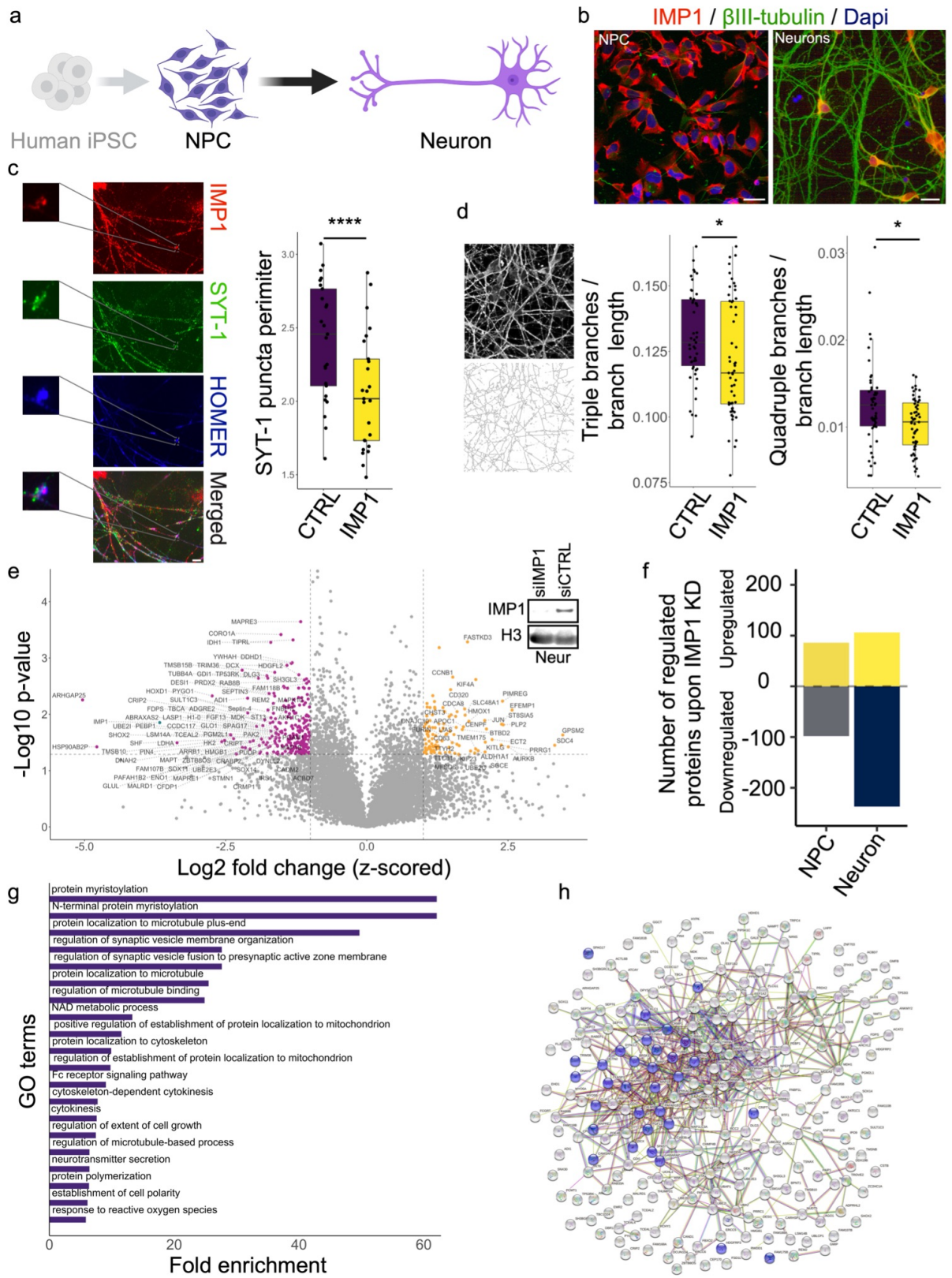

Fig. 1 | IMP1 regulates human neural proteome governing the morphological changes happening during differentiation

a, Schematic showing differentiation strategy for human neurogenesis from iPSC using a previously described protocol [31].
b, Representative confocal images of human iPSCs differentiated into neurons immunostained for IMP1, βIII-tubulin and nuclei labelled with Dapi at NPC and neuronal stages. Scale bar, 20 µm.
c, Left - representative VT-iSIM image of neurons immunostained for IMP1, the presynaptic marker SYT-1, the postsynaptic marker Homer-1 (HOMER) and nuclei labelled with Dapi. Scale bar, 10 µm. Right - quantification of SYT-1 puncta perimeter (pixels) in neurons treated with IMP1 siRNA (IMP1) vs non-targeting control (CTRL). Points presented are different fields of view. Boxplot presented is the median (middle line), interquartile range and whiskers, n=2 independent iPSC lines in 2 independent experiments. P-values calculated using two-sided Mann–Whitney test ** $P < 0.0001$.
d, Left - example image of βIII-tubulin and skeletonization for branching analysis. Right - quantification of triple and quadruple branches in neuronal processes based on βIII-tubulin immunostaining and normalised to βIII-tubulin length in neurons treated with IMP1 siRNA (IMP1) vs non-targeting control (CTRL). Points presented are different fields of view. Boxplot presented is the median (middle line), interquartile range and whiskers, n=3 independent iPSC lines in 3 independent experiments. P-values calculated using two-sided Mann–Whitney test, *$P < 0.05$, **$P<0.01$.
e, Volcano plot of proteins with differential expression in neurons treated with IMP1 siRNA (siIMP1) vs non-targeting control (siCTRL). Downregulated, unchanged and upregulated proteins are shown respectively in pink, grey and orange with the following criteria: log2 FC (z-scored) < -1 or >1 (vertical dashed line), p-value < 0.05 (horizontal dashed line), one-sample Student's t-test; n = 3 independent iPSC lines for each condition. Embedded representative image of western blot showing expression of IMP1 and H3 as loading control from knockdown experiment.
f, Barplot plot showing the number of proteins upregulated or downregulated in neurons and NPC treated with IMP1 siRNA (siIMP1) vs non-targeting control (siCTRL). For downregulated proteins selection was based on log2 FC < -1, p-value < 0.05, one-sample Student's t-test, for upregulated proteins selection was based on log2 FC > 1, p-value < 0.05, one-sample Student's t-test. For neurons, n = 3 independent iPSC lines for each condition; for NPCs, n= 2 independent IPSC lines for each condition.
g, Top GO term enrichments of downregulated proteins in IMP1 siRNA treated neurons (log2 FC < -1, $P < 0.05$). Redundancy was removed using REVIGO and top 20 significantly enriched GO terms are shown. Terms are ranked based on fold enrichment. All terms presented have a false discovery rate (FDR) <0.05. Only three proteins are found in the "protein myristoylation" and "N-terminal protein myristoylation" terms; two of these are protein phosphatases.
h, STRING[2] analysis of the protein–protein interaction network from downregulated proteins in IMP1 siRNA treated neurons (log2 FC < -1, $P < 0.05$). In blue proteins belonging to the STRING GO term "microtubule-based process" are highlighted. Network protein-protein enrichment p-value < 1.0e-16.

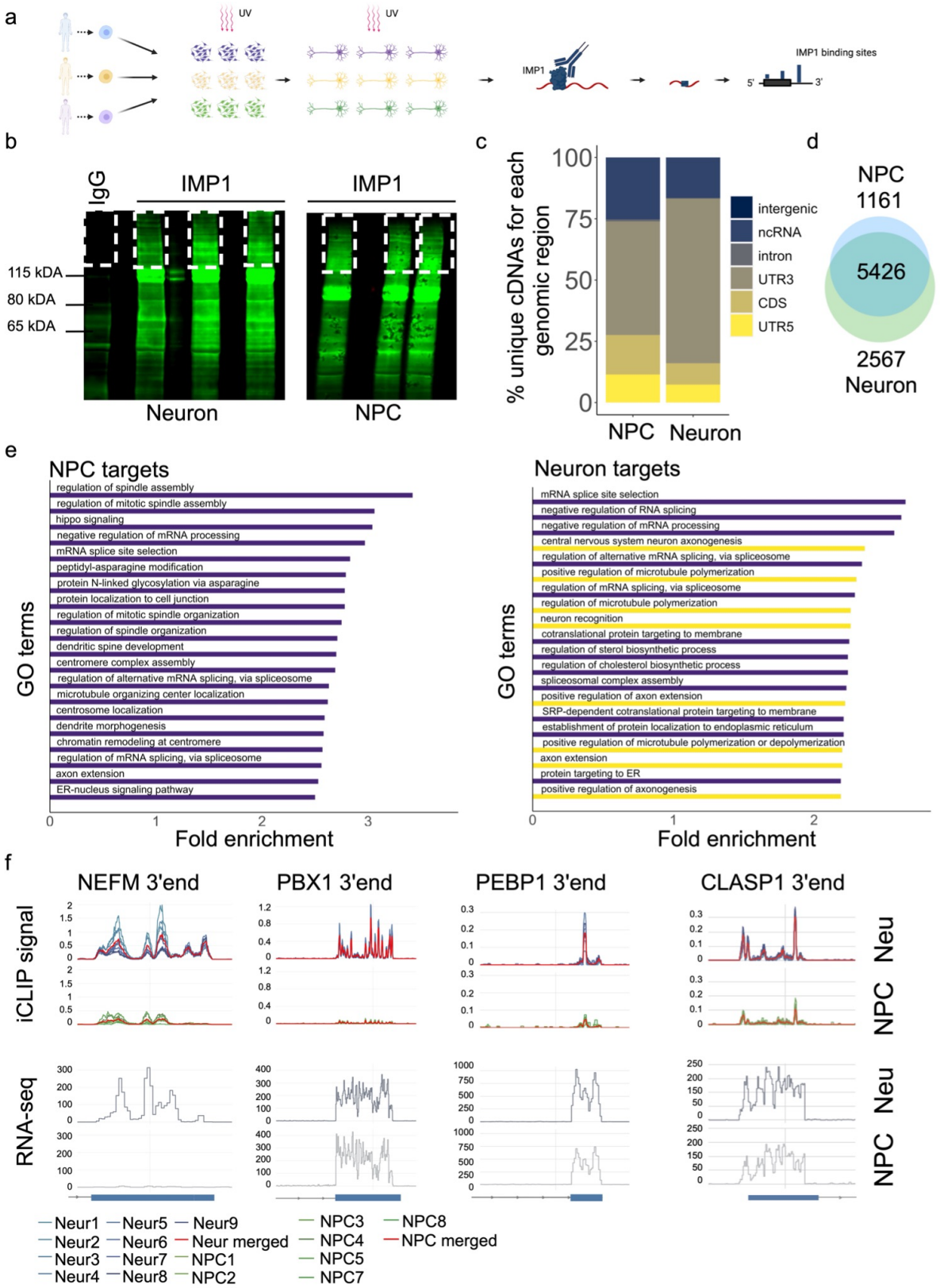

Fig. 2 | IMP1 RNA targetome is regulated during human neuronal development and reflects IMP1 cellular role

a, Schematic showing IMP1 iCLIP strategy in NPC and neurons. Briefly, cells were UV-C crosslinked, lysed and total RNA was fragmented by RNase I. IMP1-RNA complexes were immunoprecipitated (IP) and RNA was linked to an infrared dye-labeled oligo. IMP1-RNA

complexes were then run on an SDS-PAGE and transferred to a nitrocellulose membrane. RNA was visualised thanks to the IR dye and the region of interest was released from the membrane by proteinase K digestion. RNA was reverse transcribed, circularised, and PCR amplified. Three technical replicates from three independent iPSC lines were used for NPCs neurons.

b, Representative LI-Cor scanning visualisation of nitrocellulose membrane of RNA/IMP1 or RNA/IgG complexes in neurons. Visualisation is based on the infrared adaptor ligated to protein-RNA complexes. The excised portion of the membrane used to generate iCLIP libraries is shown (with dashed masks).

c, Barplot showing the percentage of unique cDNAs mapping to each region of the transcriptome for neurons and NPC. Counts were normalised to the number of genomic nucleotides corresponding to each region, and percentage of total counts were calculated. Percentage is as follows: NPC - 5'UTR 11.44, CDS 16.13, 3'UTR 46.36, Intron 0.81, ncRNA 25.13, Intergenic 0.13; MN - 5'UTR 7.32, CDS 8.71, 3'UTR 67.12, Intron 0.37, ncRNA 16.37, Intergenic 0.11

d, Venn diagram representing the overlap between genes bound by IMP1 in neurons and NPC.

e, Top GO term enrichment of genes bound by IMP1 for each cell type in neurons and NPC. Top 20 significantly enriched GO terms are shown. Terms are ranked based on fold enrichment. All terms presented have a false discovery rate (FDR) <0.05. Yellow bars highlight terms related to neurogenesis or microtubules-related pathways.

f, Mapping of IMP1 iCLIP crosslink signal (top) and RNAseq coverage signal (bottom) in neurons and NPC. For iCLIP - tracks signal for each replicate either in blue for neurons or green for NPC and the merge of all replicates in red are shown.

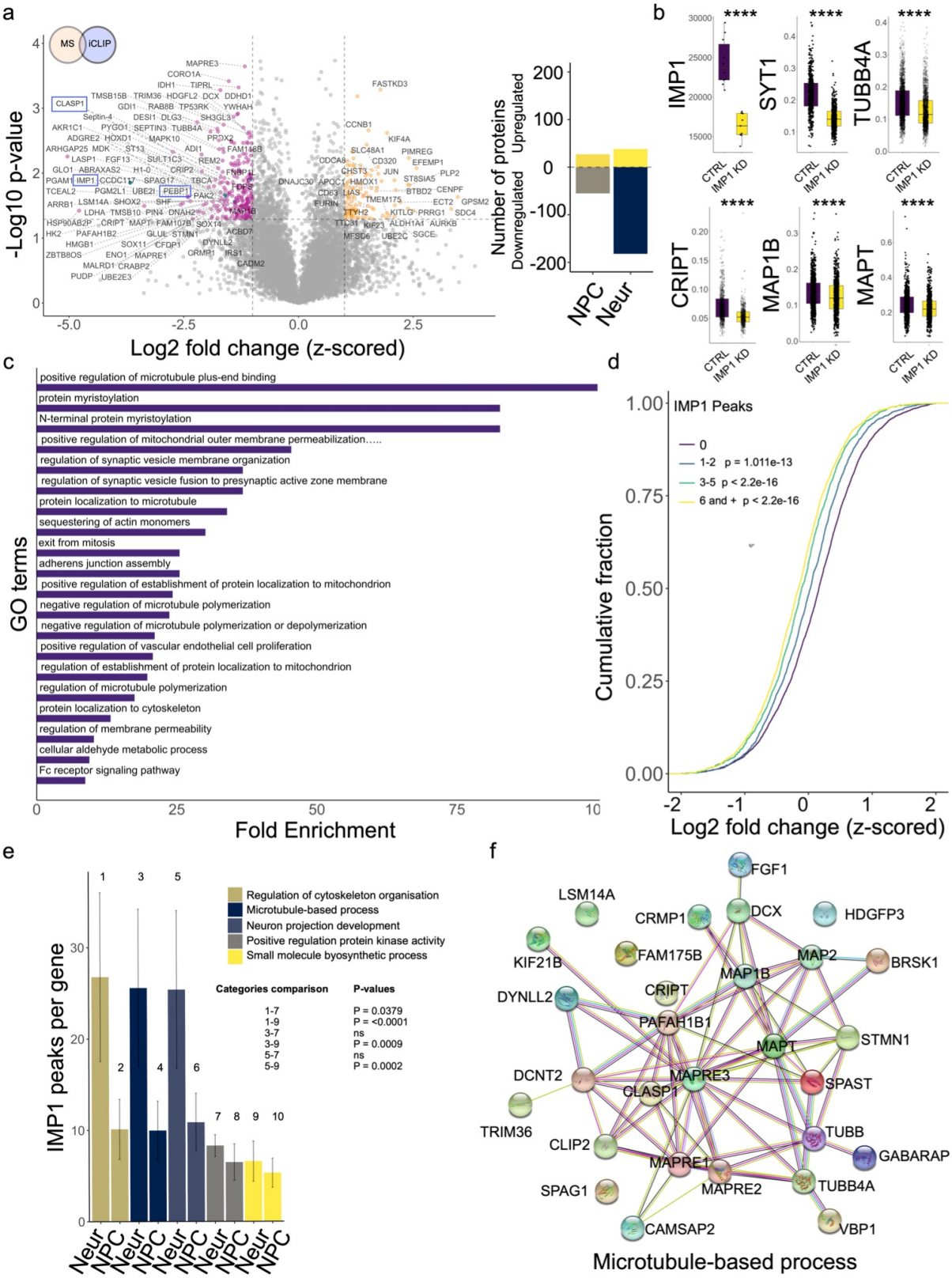

Fig. 3 | IMP1 favours microtubule protein expression by binding to corresponding RNA

a, Left - Volcano plot of proteins with differential expression in neurons treated with IMP1 siRNA vs non-targeting control (detected by MS) for IMP1 bound transcripts only (detected by iCLIP). Downregulated, unchanged and upregulated proteins are shown respectively in

pink, grey and orange. IMP1, CLASP1 and PEBP1 are highlighted with blue dots and blue squares. Right - Barplot plot showing the number of proteins upregulated or downregulated in neurons and NPC treated with IMP1 siRNA vs non-targeting control (detected by MS) for IMP1 bound transcripts only (detected by iCLIP). For downregulated proteins selection was based on log2 FC < -1, p-value < 0.05, one-sample Student's t-test, for upregulated proteins selection was based on log2 FC > 1, p-value < 0.05, one-sample Student's t-test, for transcripts containing at least one IMP1 binding site. For MS, n=3 independent iPSC lines for each condition for neurons and n=2 independent iPSC lines for each condition for NPCs; for iCLIP, n=3 technical replicates from 3 independent iPSC lines for neurons, and n=6 biological+technical replicates for NPCs.
b, Quantification from IMP1, CRIPT, SYT1, TUBB4A, MAP1B, MAPT protein expression from immunostaining on neurons treated with non-targeting control siRNA (CTRL) or IMP1 siRNA (IMP1 KD). Points presented are the mean cytoplasmic intensity per field. Boxplot presented is the median (middle line), interquartile range and whiskers, n=3 independent iPSC lines in 3 independent experiments. P-values calculated using two-sided Mann–Whitney test, **** P <0.0001
c, Top GO term enrichments of downregulated proteins in siRNA treated neurons log2 FC < -1, p-value < 0.05) for IMP1 bound transcripts detected by iCLIP. Redundancy was removed using REVIGO and top 20 significantly enriched GO terms are shown. Terms are ranked based on fold enrichment. All terms presented have a false discovery rate (FDR) <0.05.
d, Cumulative distribution plot of log2 FC in protein expression between IMP1 KD and control in neurons detected by MS was plotted for corresponding RNA classified by the number of IMP1 peaks detected by iCLIP. For MS, n=3 independent iPSC lines for each condition; for iCLIP, n=3 technical replicates from 3 independent iPSC lines. P-values were calculated using a two-sided Kolmogorov–Smirnov test comparing 1-2 peaks, 3-5 peaks or 6 and + peaks to 0 peaks. P-values are reported on the graph.
e, Number of IMP1 peaks per gene regions detected by iCLIP for GO categories related to microtubules, neuronal or other pathways classified by PANTHER - "Regulation of cytoskeleton organisation", "Microtubule-based process", "Neuron projection development", "Positive regulation protein kinase activity", "Small molecule biosynthetic process". Number of genes in each category is in the same range (between 26 and 30). Data presented is the mean +/- SEM. Each category is represented by a number above the corresponding bar. P-values calculated using a two-sided Mann–Whitney test and added to the plot. Comparison for the same cell type was performed.
f, STRING analysis of protein–protein interaction network on downregulated proteins (log2 FC < -1, P < 0.05) in IMP1 siRNA treated neurons compared to control siRNA for IMP1 bound transcripts. The GO category represented is "microtubule-based process" as classified by PANTHER.

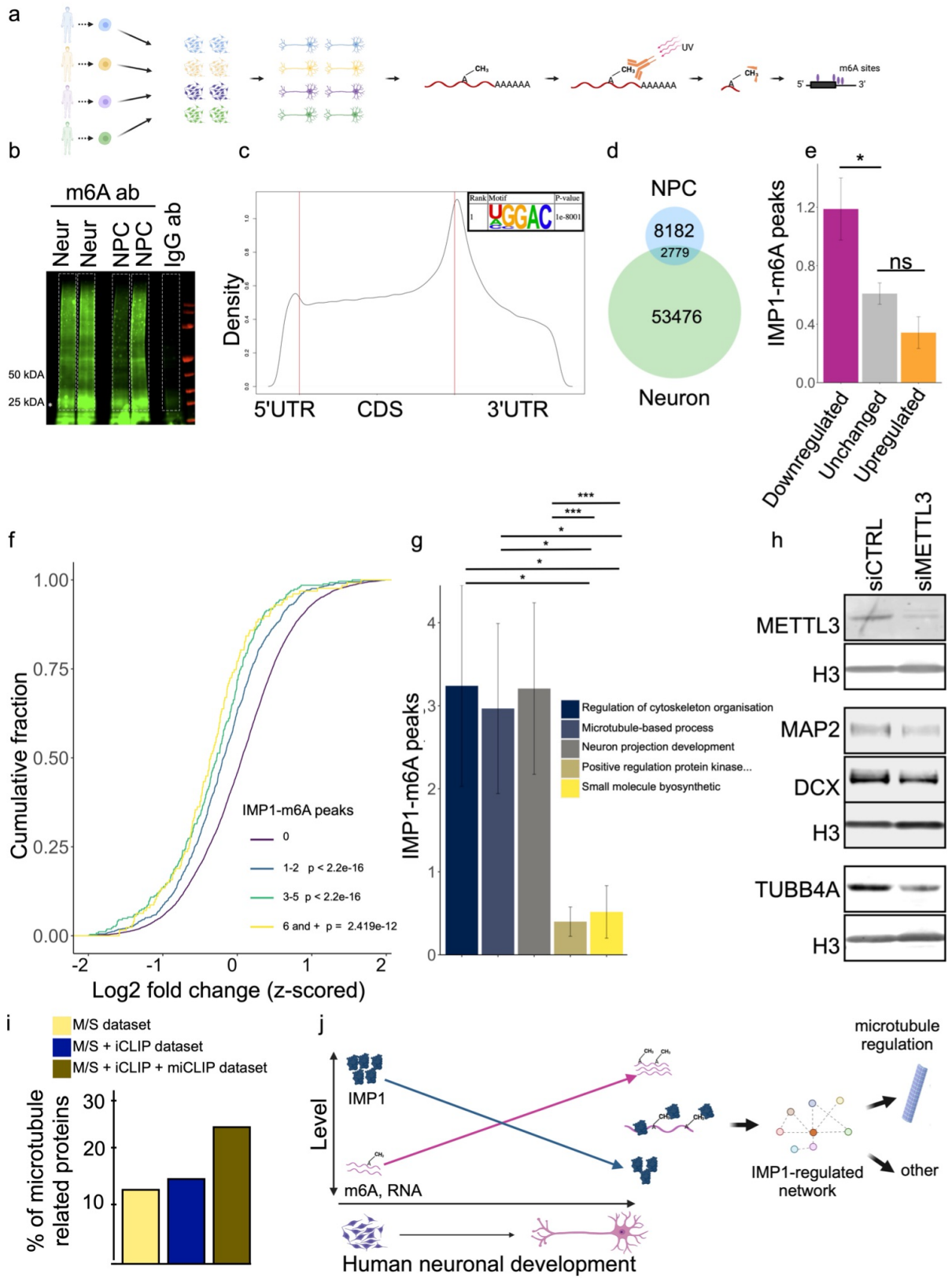

Fig. 4 | IMP1 binding to m6A largely contributes to microtubule network expression
a, Schematic showing miCLIP strategy in NPC and neurons. Briefly, poly(A)+ RNA was extracted and UV-C crosslinked to an m6A antibody (m6A ab). RNA was then fragmented by RNase I, m6A ab-mRNA complexes were immunoprecipitated (IP) and RNA was linked to an infrared dye-labeled oligo. Complexes were run on an SDS-PAGE and transferred to a

nitrocellulose membrane. RNA was visualised using the IR dye and the region of interest was released from the membrane by proteinase K digestion. RNA was reverse transcribed, circularised, and PCR amplified. Two technical replicates from four independent iPSC lines were used for NPCs and neurons.
b, Representative LI-Cor scanning visualisation of nitrocellulose membrane of poly(A)+ RNA crosslinked to an m6A antibody or IgG in neurons. Visualisation uses the infrared adaptor ligated to antibody-m6A RNA complex. The excised portion of the membrane used to generate miCLIP libraries is shown (dashed white masks)
c, Metagene plot showing m6A sites distribution in neurons. Embedded - consensus motif from HOMER motif discovery tools. Motif with best p-value is shown.
d, Venn diagram representing the number of overlapping m6A sites between neurons and NPCs.
e, Number of IMP1-m6A peaks detected by overlap between miCLIP and iCLIP for downregulated, upregulated, or unchanged proteins - respectively log2 FC < -1 in pink; -1 > log2 FC< 1 in grey; log2 FC > -1 in orange - from knockdown experiments in neurons (see Fig. 3a). Data presented is the mean +/- SEM. For MS, n=3 independent iPSC lines for each condition, for iCLIP, n=3 technical replicates from 3 independent iPSC lines and for miCLIP, n=2 technical replicates from 4 independent iPSC lines. P-values calculated using Kruskal–Wallis with Dunn's multiple comparisons test, *P < 0.05, ns = not significant.
f, Cumulative distribution plot of the log2 FC in protein expression between IMP1 knockdown and control neurons detected by MS was plotted for corresponding RNA classified by the number of IMP1-m6A peaks detected by iCLIP and miCLIP. For MS, n=3 independent iPSC lines for each condition; for iCLIP, n=3 technical replicates from 3 independent iPSC lines, for miCLIP, n=2 technical replicates from 4 independent iPSC lines. P-values calculated using two-sided Kolmogorov–Smirnov test comparing 1-2 peaks or 3-5 peaks or 6 and + peaks to 0 peaks. P-values are reported on the plot.
g, Number of IMP1-m6A peaks detected by overlap between miCLIP and iCLIP for GO categories related to microtubules, neuronal or other pathways classified by PANTHER - "Regulation of cytoskeleton organisation", "Microtubule-based process", "Neuron projection development", "Positive regulation protein kinase activity", "Small molecule biosynthetic process". Number of genes in each category is in the same range (between 26 and 30). Data presented is the mean +/- SEM. For iCLIP, n=3 technical replicates from 3 independent iPSC lines, for miCLIP, n=2 technical replicates from 4 independent iPSC lines. Data presented is the mean +/-SEM. P-values calculated using a two-sided Mann–Whitney test, * P < 0.05, *** P < 0.001.
h, Western blot analysis showing expression of IMP1, METTL3, TUBB4A, DCX, MAP2 and H3 as loading control in neurons treated with non-targeting control siRNA (siCTRL) or siRNA targeting METTL3 (siMETTL3). Representative image from 2 independent experiments performed on three technical replicates from 2 independent iPSC lines.
i, Barplot of the percentage of proteins belonging to the "microtubules-based process" terms as defined by PANTHER GO classification for each of the following category : downregulated proteins as defined by MS (log2 FC < -1 and p-value >0.05), downregulated proteins with RNA targets directly bound by IMP1 as defined by MS and iCLIP, downregulated proteins with RNA targets directly bound by IMP1 through an m6A site as defined by MS, iCLIP and miCLIP.
j, Schematic depiction of our mechanistic working model. In summary, m6A concentration increases during human neuronal differentiation, which orchestrates IMP1 regulation of microtubules during neuronal differentiation.

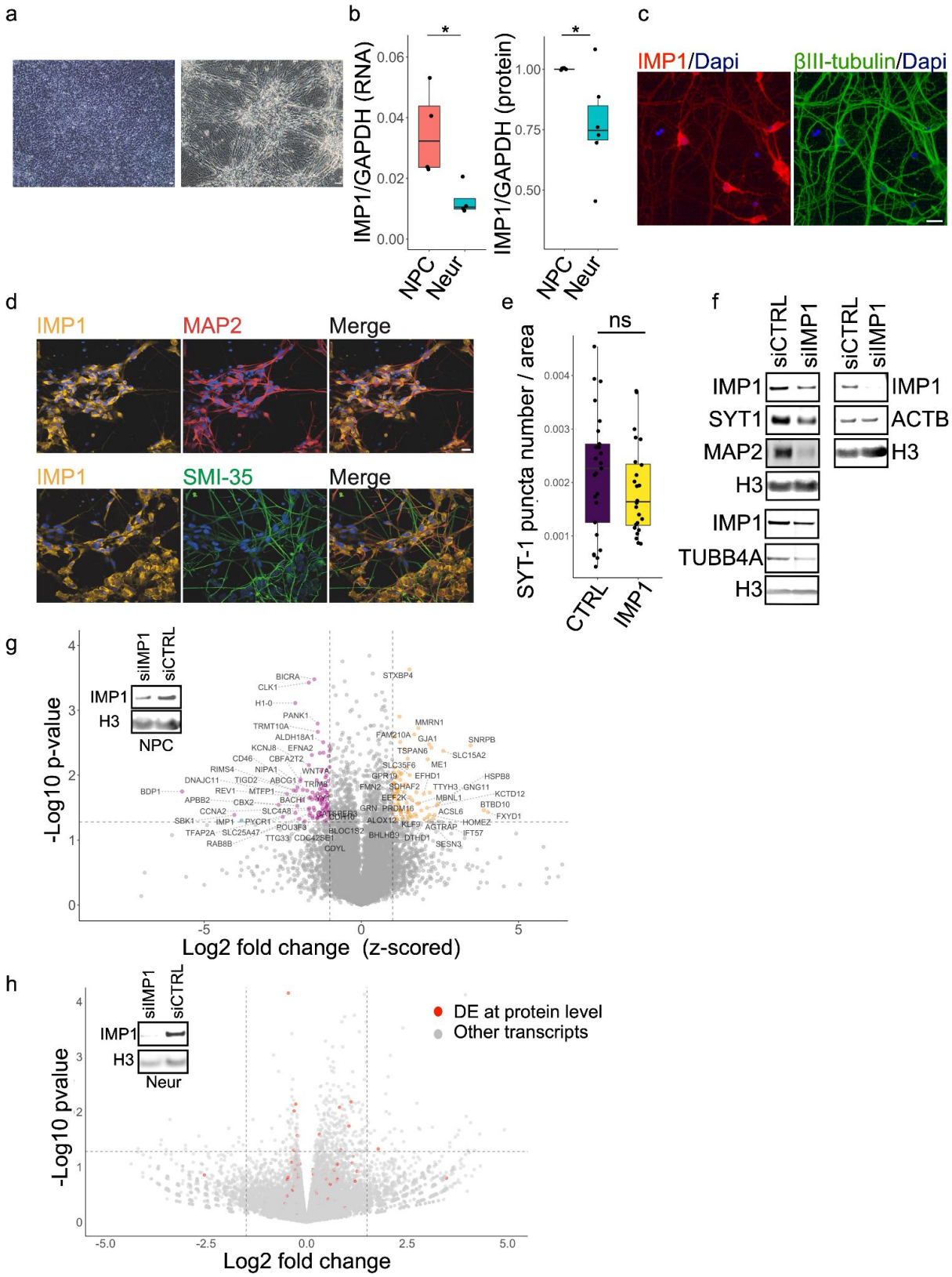

Extended Data Fig. 1 |

a, Representative light microscopy images of neuronal precursor cells - NPC (left) and neurons (right) used in this study. Scale bar, 20 µm.

b, Relative expression of IMP1 over GAPDH measured by RT-qPCR (left) and WB (right) at NPC and neuronal stages. Points presented are different biological replicates. Boxplot presented is the median (middle line), interquartile range and whiskers. For qPCR experiment n=4 independent iPSC lines, p-values calculated using P-values calculated using a two-sided Mann–Whitney test, * P <0.05. Data presented is the mean +/-SEM. For WB experiment n= 6 technical replicates from 4 independent iPSC lines in 2 independent experiments. Neuronal values are normalised on relative expression of corresponding clones. Data presented is the mean +/-SEM. P-values calculated using a two-sided Mann–Whitney test, * P <0.05.
c, Representative confocal images of neurons immunostained for IMP1 or βIII-tubulin with nuclei labelled with Dapi. Scale bar, 20 µm.
d, Representative confocal image of neurons immunostained for IMP1, MAP2 and nuclei labelled with Dapi (top row) ; IMP1, βIII-tubulin, SMI-35 and nuclei labelled with Dapi (bottom row). Scale bar, 20 µm.
e, Quantification of the number of SYT-1 puncta per area of βIII-tubulin area neurons treated with non-targeting control siRNA (CTRL) or siRNA targeting IMP1 (IMP1). Points presented are different fields of view. Boxplot presented is the mean +/-SEM, n=2 independent iPSC lines in 2 independent experiments. P-values calculated using two-sided Mann–Whitney test, ns = not significant.
f, Representative images of western blot showing expression of IMP1, SYT1, ACTB, MAP2 and H3 and IMP1, TUBB4A and H3 as loading control in neurons treated with non-targeting control siRNA (siCTRL) or siRNA targeting IMP1 (siIMP1).
g, Volcano plot of proteins with differential expression in NPCs treated with IMP1 siRNA (siIMP1) vs non-targeting control (siCTRL). Downregulated, unchanged and upregulated proteins are shown respectively in pink, grey and orange with the following criteria: log2 FC (z-scored) < -1 or >1 (vertical dashed line), p-value < 0.05 (horizontal dashed line), one-sample Student's t-test; n =2 independent iPSC lines for each condition. Embedded representative image of western blot showing expression of IMP1 and H3 as loading control from knockdown experiment.
h, Volcano plot of genes with differential expression in IMP1 knockdown vs control neurons for RNAseq experiment. Transcripts which correspond to differentially expressed proteins detected by MS are shown in red. Vertical dashed lines indicate cut-off of log2 FC (1.5 or -1.5), the horizontal dashed lines indicate cut-off of p-value (0.05); n = 3 independent iPSC lines for each condition. Embedded - representative image of western blot showing expression of IMP1, and H3 as loading control from knockdown experiment

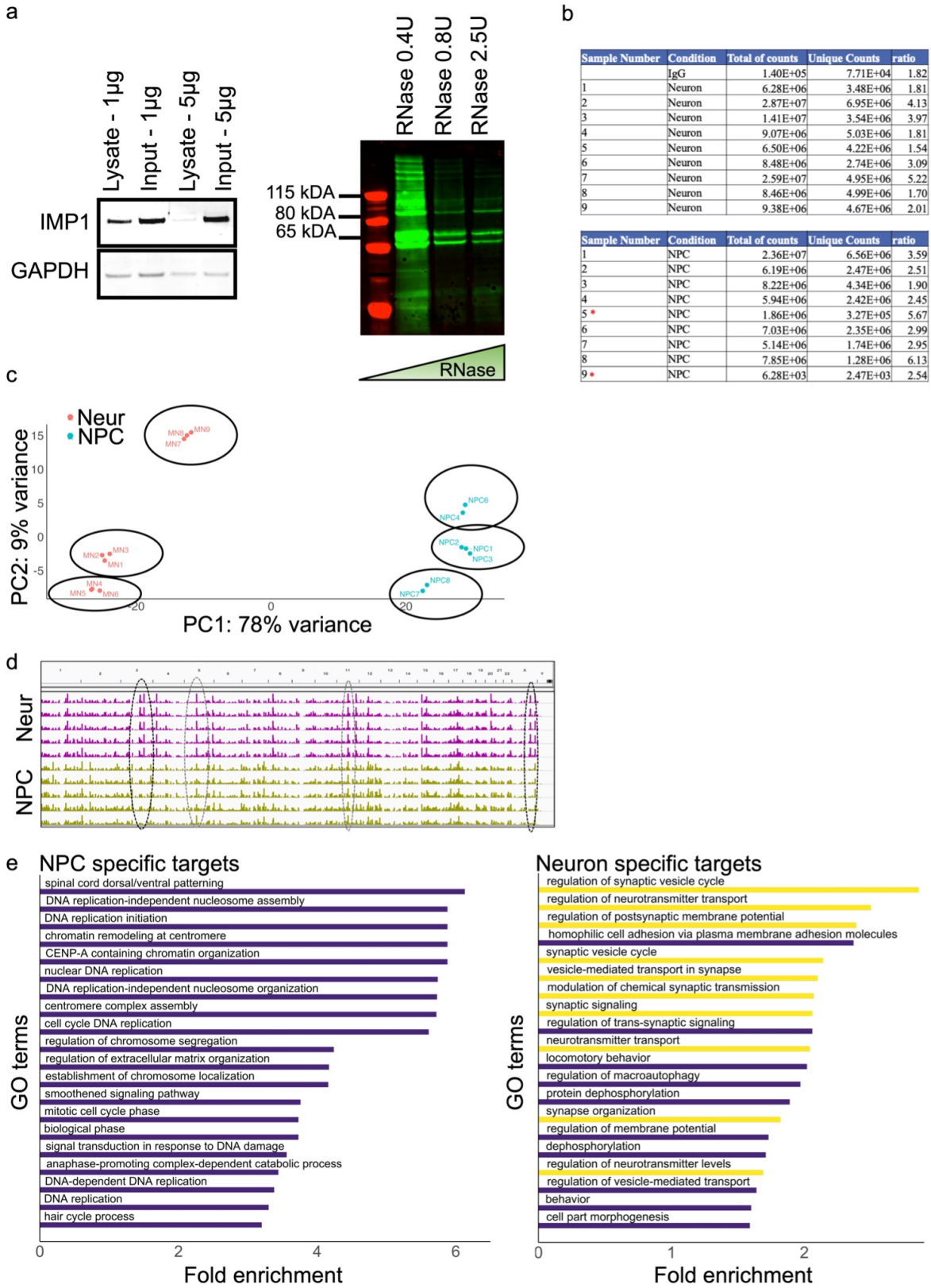

Sample Number	Condition	Total of counts	Unique Counts	ratio
	IgG	1.40E+05	7.71E+04	1.82
1	Neuron	6.28E+06	3.48E+06	1.81
2	Neuron	2.87E+07	6.95E+06	4.13
3	Neuron	1.41E+07	3.54E+06	3.97
4	Neuron	9.07E+06	5.03E+06	1.81
5	Neuron	6.50E+06	4.22E+06	1.54
6	Neuron	8.48E+06	2.74E+06	3.09
7	Neuron	2.59E+07	4.95E+06	5.22
8	Neuron	8.46E+06	4.99E+06	1.70
9	Neuron	9.38E+06	4.67E+06	2.01

Sample Number	Condition	Total of counts	Unique Counts	ratio
1	NPC	2.36E+07	6.56E+06	3.59
2	NPC	6.19E+06	2.47E+06	2.51
3	NPC	8.22E+06	4.34E+06	1.90
4	NPC	5.94E+06	2.42E+06	2.45
5 *	NPC	1.86E+06	3.27E+05	5.67
6	NPC	7.03E+06	2.35E+06	2.99
7	NPC	5.14E+06	1.74E+06	2.95
8	NPC	7.85E+06	1.28E+06	6.13
9 *	NPC	6.28E+03	2.47E+03	2.54

Extended Data Fig. 2 |

a, Left - Western blot validation of IMP1 immunoprecipitation antibody concentration for iCLIP experiment. A concentration of 1µg and 5µg of antibody per 1 mg of protein lysate was tested. GAPDH immunostaining was used as a loading control. Right - representative LI-Cor scanning visualisation of nitrocellulose membrane of RNA/IMP1 complexes in neurons

treated with a gradient of RNAse concentration - 0.4, 0.8 and 2.5U per 1 mL of lysate at a protein concentration of 1 mg/ml. Visualisation uses the infrared adaptor ligated to RNA.
b, Table indicating the number of total reads, unique reads and ratio of both for each iCLIP sample. IgG condition was used as negative technical control. Red asterixis show samples excluded from further analysis because of a significantly lower number of unique counts compared to other samples.
c, Principal component analysis (PCA) of cDNA counts from iCLIP experiment of each neuron and NPC samples. Technical replicates for each clone are circled.
d, Mapping tracks of iCLIP crosslink signals on the whole transcriptome visualised using Integrative Genomics Viewer software for five neurons and five NPC samples, respectively in pink and yellow. Dotted oval highlights similar (dark grey) and dissimilar (light grey) genomic crosslink regions between NPC and neurons.
e, Top GO term enrichments of IMP1 uniquely bound genes in neurons or NPCs. Top 20 significantly enriched GO terms are shown. Terms are ranked based on fold enrichment. All terms presented have a false discovery rate (FDR) <0.05. Yellow bars highlight terms related to neurogenesis pathways.

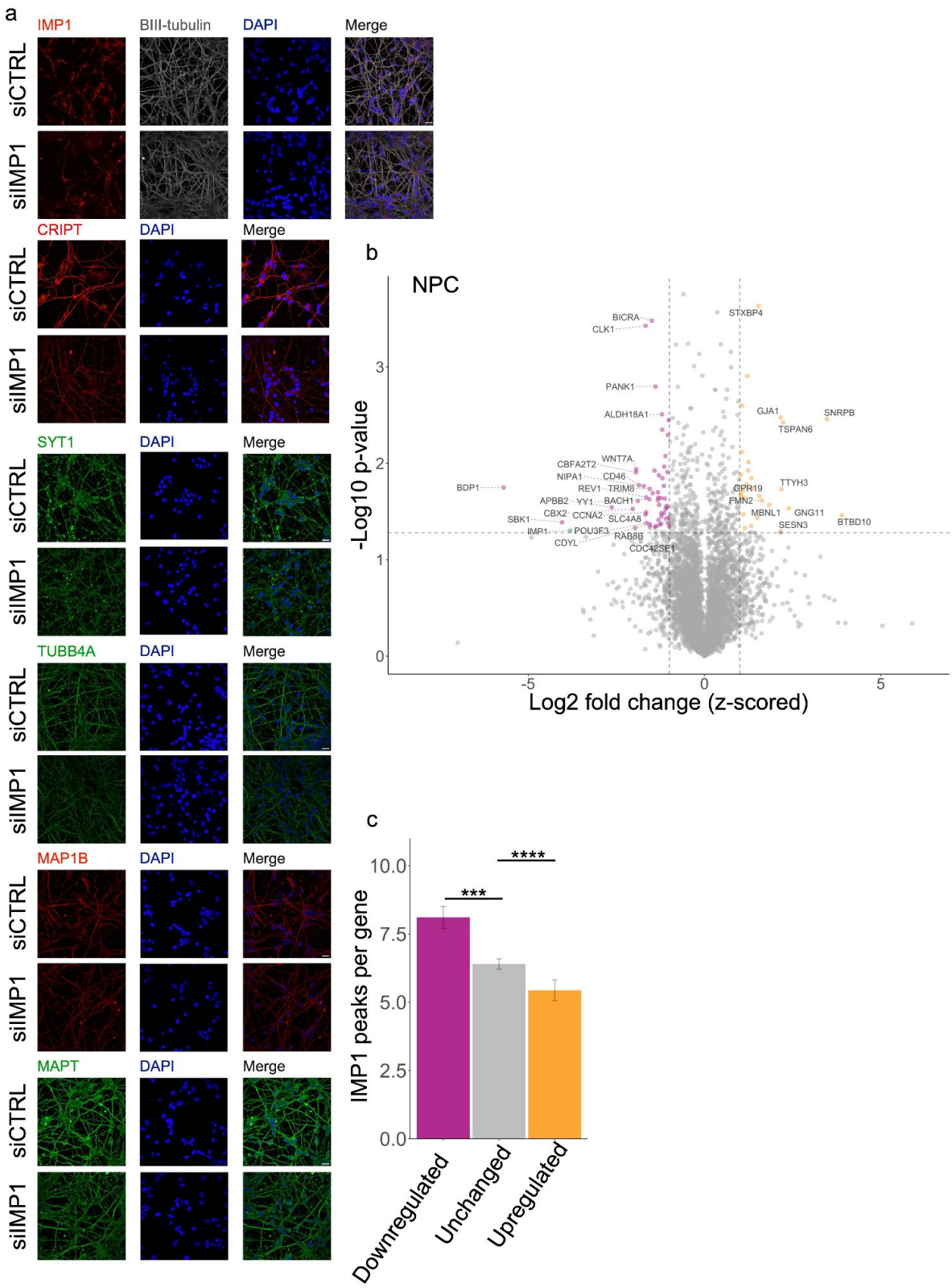

Extended Data Fig.3 |

a, Representative confocal images of neurons treated with siRNA control or siRNA IMP1 and immunostained for IMP1, CRIPT, SYT1, TUBB4A, MAP1B or MAPT together with Dapi staining. Scale bar, 20 µm.

b, Volcano plot of proteins with differential expression in NPC treated with IMP1 siRNA vs non-targeting control (detected by MS) for IMP1 bound transcripts only (detected by iCLIP).

Downregulated, unchanged and upregulated proteins are shown respectively in pink, grey and orange. For downregulated proteins selection was based on log2 FC < -1, p-value < 0.05, one-sample Student's t-test, for upregulated proteins selection was based on log2 FC > 1, p-value < 0.05, one-sample Student's t-test, for transcripts containing at least one IMP1 binding site. For MS, n=2 independent iPSC lines for each condition; for iCLIP, n=6 technical + biological replicates.

c, Number of IMP1 peaks per gene detected by iCLIP for downregulated, upregulated, or unchanged proteins - respectively log2 FC < -1, -1 > log2 FC < 1, log2 FC > 1 - from knockdown experiments in neurons detected by MS (see Fig. 3a). Data presented is the mean +/- SEM. For MS, n=3 independent iPSC lines for each condition; for iCLIP, n=3 technical replicates from 3 independent iPSC lines. Kruskal–Wallis with Dunn's multiple comparisons test,*** P < 0.001, **** P < 0.0001.

a

Sample Number	Condition	Total of counts	Unique Counts	ratio
	no_XL	5.05E+06	2.51E+06	2.01
1	Neuron	2.21E+06	3.52E+05	6.29
2	Neuron	5.50E+06	2.40E+06	2.29
3	Neuron	1.01E+07	4.82E+06	2.11
4 *	Neuron	3.00E+06	2.58E+05	11.61
5	Neuron	7.82E+06	2.70E+06	2.89
6	Neuron	2.50E+06	1.31E+06	1.90
7	Neuron	2.62E+07	1.05E+07	2.49
8	Neuron	2.84E+07	1.15E+07	2.48
Sample Number	**Condition**	**Total of counts**	**Unique Counts**	**ratio**
1 *	NPC	1.63E+05	1.60E+04	10.17
2	NPC	4.00E+06	2.58E+05	15.48
3	NPC	2.02E+06	8.90E+05	2.27
4	NPC	1.95E+06	4.99E+05	3.90
5	NPC	2.90E+06	1.21E+06	2.40
6	NPC	2.24E+06	1.06E+06	2.12
7	NPC	4.63E+06	1.53E+06	3.03
8	NPC	7.31E+06	2.35E+06	3.12

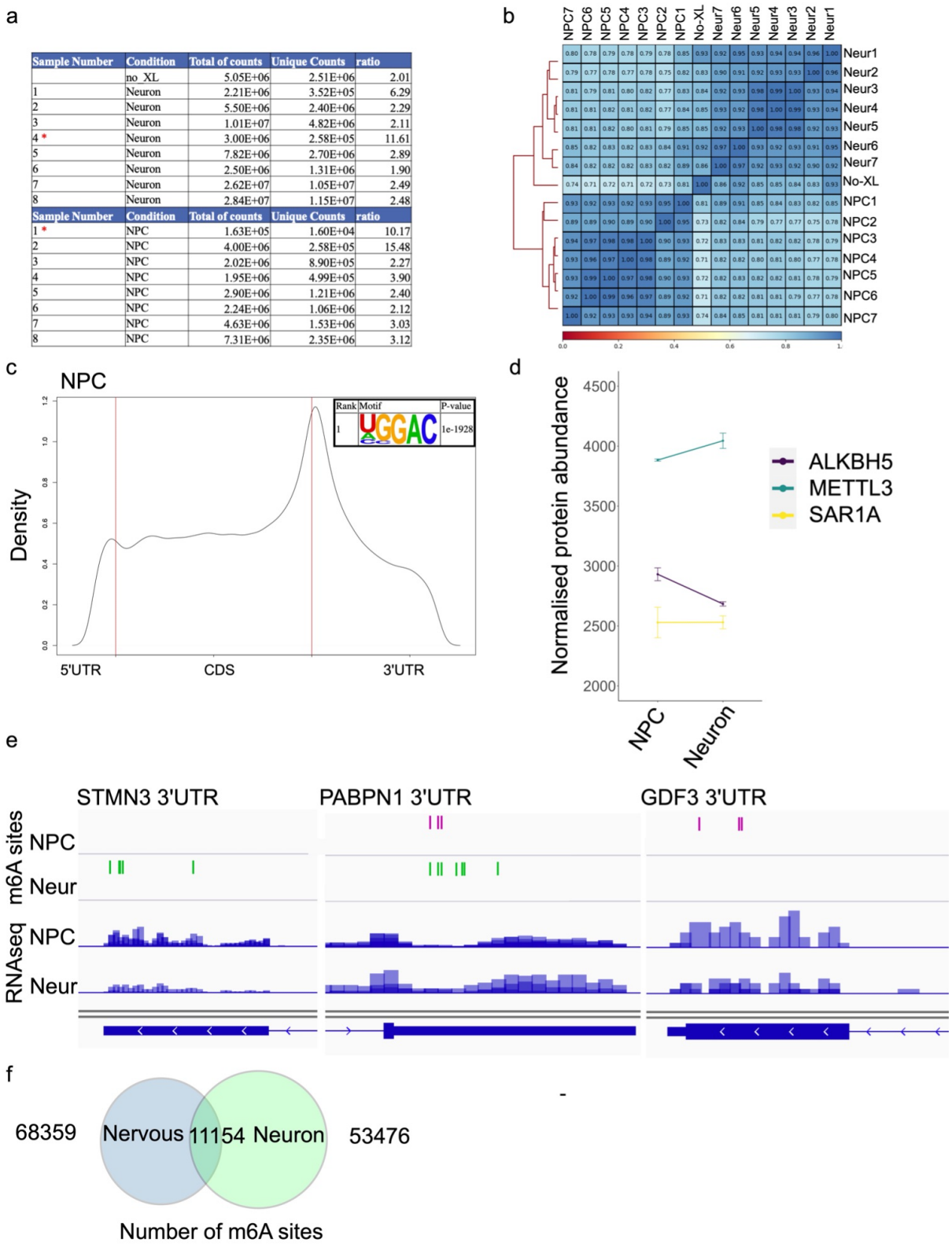

Extended Data Fig. 4 |

a, Table indicating the number of total reads, unique reads and ratio of both for each miCLIP sample. Non crosslinked and IgG conditions were used as negative technical controls (only the non-crosslinked condition was sequenced due to the absence of cDNA being generated in the IgG condition). Red asterixis show samples excluded from further analysis because of

a significantly lower number of unique counts and/or high ratio of unique reads over total reads compared to other samples.
b, Heatmap of correlation matrix for read coverage of binned genomics regions for each NPC, neuron, and non-crosslinked samples. The coloured scale depicts the correlation values which are also indicated in each square. The y-axis on the left side shows the hierarchical clustering of the samples.
c, Metagene plot showing m6A residue distribution in NPC. Embedded - consensus motif from HOMER motif discovery tools. Motif with best p-value is shown.
d, Abundance level of different proteins detected by MS in NPC and neurons treated with siRNA CTRL. Expression was normalised based on the summed abundances per sample, n=2 independent iPSC lines.
e, Mapping tracks of m6A sites detected by miCLIP (top) and RNAseq coverage signal (bottom) in neurons and NPC. The 3'UTR of three different genes is visualised using Integrative Genomics Viewer (IGV) software.
f, Venn diagram representing the overlap of m6A sites between neurons and a meta-analysis of published RNA methylation datasets (see method).

Methods

Ethics statement

Informed consent was obtained from healthy control subjects in this study. Experimental protocols were all carried out according to approved regulations and guidelines by UCLH's National Hospital for Neurology and Neurosurgery and UCL's Institute of Neurology joint research ethics committee (09/0272).

Cell culture

All cell cultures were maintained at 37°C and 5% CO_2. The hIPSC were cultured on Geltrex (Life Technologies) coated plates with Essential 8 Medium (Life Technologies) and passaged using 0.5 mM EDTA (Life Technologies). hIPSC-derived NPCs and neurons were cultured and differentiated according to previously published protocol[32]. Briefly, hiPSCs were first differentiated by plating to 100% confluency in medium consisting of DMEM/F12 Glutamax, Neurobasal, L-Glutamine, N2 supplement, non-essential amino acids, B27 supplement, β-mercaptoethanol (all from Life Technologies) and insulin (Sigma). Treatment with small molecules from day 0–7 was as follows: 1 μM Dorsomorphin (Millipore), 2 μM SB431542 (Tocris Bioscience), and 3.3 μM CHIR99021 (Miltenyi Biotec). At day 4 and 11, the cell layer was enzymatically dissociated using 1mg/ml of dispase (GIBCO) and plated in one in two onto geltrex coated plates media containing 1 μM Rock Inhibitor (Tocris Bioscience 1254/10). From day 8 cell were patterned for 7 days with 0.5 μM retinoic acid and 1 μM Purmorphamine. At day 14 were treated with 0.1 μM Purmorphamine for a further 4 days to generate spinal cord neurons precursors (NPCs). NPCs were either expanded or terminally differentiated with 0.1 μM Compound E (CE) (Enzo Life Sciences) to promote cell-cycle exit. For all experiments cells were harvested at the NPC stage or mature neurons stage (day 7 post CE treatment). Details of the lines used in this study are provided in Table 1. Two of the control lines used (control 2 and control 3) are commercially available and were purchased from Coriell (ND41866*C) and Thermo-Fisher Scientific (A18945) respectively.

Primary antibodies

Rabbit anti-IMP1 (MBL, RN007P), rabbit anti-IgG (Proteintch 30000-0-AP), mouse anti-Actb (Sigma, A2228), rabbit anti-H3 (Abcam EPR17785), chicken anti-Homer-1 (Synaptic System, 160006), mouse anti-Synaptotagmin1 (Synaptic System, 105011), mouse anti-SMI-35 (Biolegend, 835603), rabbit anti-MAP1B (Proteintech, 21633-1-AP), mouse anti-MAP2 (Abcam ab11267), chicken anti-MAP2 (Abcam ab5392), chicken anti-beta III tubulin (Abcam, ab41489), mouse anti-beta IV tubulin (Abcam, ab11315), rabbit anti-DCX (Proteintech, 13925-1-AP), rabbit anti-MAPRE2 (Proteintech 10364-1-AP), rabbit anti-Stathmin1 (Proteintech ,11157-1-AP), mouse anti-MAPT(ab80579), rabbit anti-CRIPT (Proteintech ,11211-1-AP), mouse anti-m6A (Abcam, ab151230), rabbit anti-METTL3 (Proteintech r15073-1-AP).

Immunofluorescence staining

Cells were fixed in 4% paraformaldehyde in PBS for 10 min at room temperature. For permeabilization and non-specific antibody blocking, 0.3% Triton-X containing 5% bovine serum albumin (BSA) (Sigma) in PBS was added for 60 min. Primary antibodies were made up in 5% BSA and then applied overnight at 4°C. After three washes with PBS, species-specific Alexa Fluor-conjugated secondary antibody (Life Technologies) at 1:1000 dilution in 5% PBS-BSA was applied in the dark for 60 min. Cells were washed once in PBS containing Dapi, 4′,6-diamidino-2-phenylindole nuclear stain (1:1000) for 10 min. Images were taken using the Zeiss invert 880 confocal microscope or the VT-iSIM.

Immunofluorescence quantification

For immunofluorescence quantification a maximum projection of the images was taken from the Z stack. Using CellProfiler [33] the nuclei were then filtered to remove dead cells. The nuclear mask was expanded by 15 pixels and this region was defined as the cytoplasm. To define the neurites, a mask was created from βIII-tubulin, with the nuclei and cytoplasmic compartments removed. The mean intensities for each compartment were calculated, using the defined masks. For synaptic particle quantification, thresholding was used to define SYT1 particles. The particles were then quantified and the area measured. For branching analysis, the maximum projection of βIII-tubulin underwent pre-processing to remove noise and binarization and then skeletonised using the Skeletonize3D plugin for ImageJ. The AnalyseSkeleton plugin was then used for branch quantification.

Western blotting

Cells were washed with cold PBS 1X on ice and sonicated in RIPA buffer (25 mM Tris-HCl pH 7.6, 150 mM NaCl, 1% NP-40, 1% sodium deoxycholate, 0.1% SDS) supplemented with 1X Protease Inhibitor Cocktail (Complete, Roche Diagnostics). Supernatants were cleared of debris by 15 min centrifugation at 13000 rpm at 4°C. Protein quantification was performed using the Pierce BCA protein assay kit according to the manufacturer's instruction (Thermo Fisher Scientific, 23227). Equal quantities of proteins were supplemented with 4x Nupage loading buffer containing 1mM DTT and incubated at 90°C for 10 minutes. Samples were separated onto 4–12% Bis–Tris protein gels (Invitrogen) in 1X MES buffer (Invitrogen) and transferred onto a nitrocellulose membrane for 1 h at constant 30 V at 4°C using wet transfer (Invitrogen). Membranes were blocked by incubation in 5% milk in PBS, for IMP1 staining for 1 h at room temperature under agitation or in 5% milk in PBS-0.05% Tween-20 (PBS-T) for all other staining. Membranes were then incubated with primary antibodies ON at 4°C in 1% milk in PBS for anti-IMP1 antibody or in 2.5% milk in PBS-T for all other antibodies either 1h at RT or ON at 4°C. Membranes were extensively washed in PBS-T and then incubated with

LI-COR species-specific secondary antibodies (IRdye680 1:15000, IRdye800 1:15000) at room temperature for 1h. Unbound secondary antibody was washed in PBS-T 1X three times. Blots were imaged by Odyssey scanning (LI-COR) and quantified using Fiji software [34].

siRNA knockdown

For RNAseq and proteomics experiments NPCs were plated in 12-well (RNAseq) or 6-well plates (proteomics) in N2B27 media at a density of 2.5 x 10^5 cells/well or 2.5 x 10^6 cells/well respectively. They were transfected the next day with siRNA directed against IMP1/IGF2BP1 (ON-TARGETplus SmartPool L-003977-00-0005 siRNA, Horizon) or non-targeting siRNAs as negative control (ON-TARGETplus Non-targeting Control Pool, D-001810-10-05, Horizon). A concentration of 30 pmol for 12-well plate and 300 pmol for 6-well plate for IMP1 was used. For m6A validation effect on protein expression, NPCs were plated in 12-well in N2B27 media at a density of 2.5 x 10^5 cells/well. They were transfected the next day with siRNA directed against METTL3 (L-005170-02-0005,siRNA, Horizon) or non-targeting siRNAs as negative control (ON-TARGETplus Non-targeting Control Pool, D-001810-10-05, Horizon) with 10 pmol. Lipofectamine RNAiMax (ThermoFisher Scientific) was used as a transfection reagent according to the manufacturer's instructions. After overnight incubation, the media was changed to FGF in N2B27 to maintain cells at the NPC stage or 0.1 µM Compound E in N2B27 to allow terminal differentiation to neurons. Samples were harvested for either protein or RNA extraction at 6 days after media change. Knock-down efficiency was systematically assessed by WB.

RNA extraction for sequencing

IMP1 and control siRNA treated NPC and neurons were washed with PBS 1X and harvested by centrifugation. Total RNA was extracted using Maxwell RSC simplyRNA cells kit including DNase treatment in the Maxwell RSC instrument following manufacturer’s instructions. RNA concentration and the 260/280 ratio were assessed using Nanodrop, and the Agilent 2400 Bioanalyser was used to assess quality. RNA integrity (RIN) scores were used to quality check samples.

RNA extraction for qPCR

NPC and neurons were washed with PBS 1X and harvested by centrifugation. Total RNA was extracted using Maxwell RSC simplyRNA cells kit including DNase treatment in the Maxwell RSC instrument following manufacturer’s instructions. RNA concentration and the 260/280 ratio were assessed using Nanodrop.

RNA extraction for miCLIP

NPC and neuron samples were washed with PBS 1X on ice. Content of 80 to 100% of two 6-well plate was lysed in 1.5 mL TRIzol reagent (Invitrogen, 15596206) and total RNA was extracted using manufacturer’s instruction (all volumes were scaled up according to the initial volume TRIzol). RNA was resuspended in 30µl of RNase free water. RNA concentration and the 260/280 ratio were assessed using Nanodrop, and the Agilent 2400 Bioanalyser was used to assess quality. RNA integrity (RIN) scores were used to quality check samples.

Reverse transcription and qPCR

RevertAid First Strand cDNA Synthesis kit (ThermoFisher Scientific) was used to

synthesise cDNA using 1 µg of total RNA and random hexamers. Appropriate dilution of the cDNA was then used in qPCR reactions containing PowerUp SYBR Green Master Mix (ThermoFisher Scientific) and primer pairs, using the QuantStudio 6 Flex Real-Time PCR System (Applied Biosystems). Specific amplification was determined by melt curve analysis. Gene expression levels were measured using the ΔΔCT method. IMP1 was amplified using the following pair of primers IMP1-FWD 5'-CAGGGCCGAGCAGGAAATAA -3, IMP1-REV 5'-CAGGGATCAGGTGAGACTGC -3' and normalised on GAPDH gene amplified with the following pair of primers: GAPDH-FWD 5'-ATGACATCAAGAAGGTGGTG-3', GAPDH-REV 5'-CATACCAGGAAATGAGCTTG-3'

PolyA enrichment

Total RNA was treated with DNAse I (TURBO DNAse, ambion, AM2238) using rigorous DNAse treatment conditions according to manufacturer's instructions. DNAse free Poly(A)+ RNA was prepared using oligo dt dynabeads (NEB S1419S) using the following protocol: 1mg of dynabeads were washed with binding buffer and resuspended in 100µl of binding buffer (20 mM Tris-HCl, pH 7.5, 1.0 M LiCl, 2 mM EDTA). Volume of RNA was adjusted to 100µl in RNAse free water and mixed with 100µl of binding buffer. Samples were incubated at 65°C for 2 min and immediately put on ice. RNA was thoroughly mixed with washed beads and tubes were rotating head over tail for 5 min at RT. Two washes with wash buffer A (10 mM Tris-HCl, pH 7.5 ,0.15 M LiCl, 1 mM EDTA 10 mM Tris-HCl, pH 7.5) were performed followed by elution with 50µl of elution buffer (20 mM Tris-HCl, pH 7.5, 1 mM EDTA). Samples were then incubated at 80°C for 2 min under gentle agitation and placed on a magnetics rack. Supernatant was reused for another round of purification after beads were washed with 100µl of elution buffer and 200µl of wash buffer. RNA concentration was assessed using Nanodrop.

Individual-nucleotide resolution UV-crosslinking and immunoprecipitation of protein-RNA complexes (iCLIP)

iCLIP was performed as previously described [35] with minor modifications. Briefly, three biological and three technical replicates for NPCs and neurons were cross-linked at 300mJ and then lysed in 1ml of IP lysis buffer. RNA fragmentation was performed with 0.4 units of RNase I (Thermo Scientific, EN0602) and 4µl Turbo DNase I (Ambion, AM223) added to 1mL of protein lysate at a concentration of 1mg/mL. Ideal RNAse concentration was previously determined using a concentration gradient: low (0.4U), medium (0.8U) high (2.5 U) to 1 mg of protein lysate from NPC and neuron. Ideal IMP1 antibody was previously determined using 1µg or 5µg of antibody to 1 mg of protein lysate. To separate protein-RNA complexes, samples were incubated with 5µg of anti-IMP1 antibody or 5µg of anti-IgG (negative control) coupled to Protein G beads (Dynal) at 4°C ON rotating head over tail. RNA was ligated to a pre-adenylated infrared labelled IRL3 adaptor (Zarnegar et al., 2016) with the following sequence:
/5rApp/AG ATC GGA AGA GCG GTT CAG AAA AAA AAA AAA /iAzideN/AA AAA AAA AAA A/3Bio/. The protein-RNA complexes were then size-separated by SDS-Page, blotted onto nitrocellulose and visualised by Odyssey scanning (LI-COR). Desired region (determined from the RNAse gradient experiment) was cut from the membrane in small pieces and RNA was released from the membrane by proteinase K (Roche, 03115828001) digestion and incubation at 60 min at 50°C. RNA was recovered by Phenol Chloroform precipitation. cDNA was synthesised with Superscript IV Reverse Transcriptase (Life Technologies). Reverse transcription was performed with primers containing UMIs and barcode (XXXXX) to allow

multiplexing: /5Phos/ WWW *XXXXX* NNNN AGATCGGAAGAGCGTCGTGAT /iSp18/ GGATCC /iSp18/ TACTGAACCGC. cDNA molecules were purified using AMPure XP beads (Beckman-Coulter, USA), then circularised using Circligase II (Epicenter) followed by AMPure XP beads purification. After PCR amplification, libraries were size-selected by gel-purification and size distribution was assessed using Agilent 2400 Bioanalyser. Libraries were quantified by QuBit dsDNA HS Assay. Library composed of the same quantity of cDNA for each sample was sequenced as single-end 100bp reads on Illumina HiSeq 4000.

m6A Individual-nucleotide resolution UV-crosslinking and immunoprecipitation (miCLIP)

miCLIP was performed as previously described [36] with minor modifications. Briefly, PolyA RNA (1µg) was brought to 30µl water and incubated with 3µl of 10X Fragmentation Buffer (Thermoscientific) at 60°C for 15min. Samples were immediately placed on ice and 3.3 µl of Stop Solution was added. Samples were incubated with 10µl of 1 µg/µl of anti-m6A antibody in 500µl IP buffer (50 mM Tris-HCL, pH 7.4, 100mM NaCl, 0.05% NP-40) for 2h at 4°C rotating head over tail. RNA-anti m6A antibody complexes were crosslinked in a 6-well plate on ice twice with 0.3 J/cm-2 UV light (254 nm) in a stratalinker. Negative controls (non-crosslink and anti-IgG antibodies) were also prepared. Crosslinked RNA-anti-m6A complexes were mixed with 30µl of washed Protein G Dynabeads (Dynal) and incubated at 4°C for 2 hours rotating head over tail. From this point, the library preparation steps were performed as described in the iCLIP section. The correct region from the nitrocellulose membrane was cut according to previously published protocol (Grozhik et al., 2017). Libraries were sequenced with a single-end 100bp run using an Illumina Hiseq4000 platform.

Sample preparation for proteomics analysis

Neurons and NPC pellets were lysed in 150 µL buffer containing 1% sodium deoxycholate (SDC), 100 mM triethylammonium bicarbonate (TEAB), 10% isopropanol, 50 mM NaCl and Halt protease and phosphatase inhibitor cocktail (100X) (Thermo, #78442) on ice, assisted with probe sonication, followed by heating at 90°C for 5 min and re-sonicated. Protein concentration was measured with the Quick Start Bradford Protein Assay (Bio-Rad) according to manufacturer's instructions. Protein aliquots of 50 µg were reduced with 5 mM tris-2-carboxyethyl phosphine (TCEP) for 1 h at 60°C and alkylated with 10 mM iodoacetamide (IAA) for 30 min in dark, followed by overnight digestion with trypsin at final concentration 75 ng/µL (Pierce). Peptides were labelled with the TMT 10plex reagents (Thermo) according to manufacturer's instructions. The mixture was acidified with 1% formic acid and the precipitated SDC was removed by centrifugation. Supernatant was then dried with a centrifugal vacuum concentrator.

High-pH Reversed-Phase peptide fractionation of TMT labelled peptides

Peptides were fractionated with high-pH Reversed-Phase (RP) chromatography with the XBridge C18 column (2.1 x 150 mm, 3.5 µm, Waters) on a Dionex UltiMate 3000 HPLC system. Mobile phase A was 0.1% (v/v) ammonium hydroxide and mobile phase B was acetonitrile, 0.1% (v/v) ammonium hydroxide. The TMT labelled peptides were fractionated at a flow rate of 0.2 mL/min using the following gradient: 5 minutes at 5% B, for 35 min gradient to 35% B, gradient to 80% B in 5 min, isocratic for 5 minutes and re-equilibration to 5% B. Fractions were collected every 42 sec, combined orthogonally in 12 fractions and vacuum dried.

LC-MS analysis

LC-MS analysis was performed on a Dionex UltiMate 3000 UHPLC system coupled with the Orbitrap Lumos Mass Spectrometer (Thermo Scientific). Peptides were loaded onto the Acclaim PepMap 100, 100 µm × 2 cm C18, 5 µm, trapping column at 10 µL/min flow rate and analysed with the EASY-Spray C18 capillary column (75 µm × 50 cm, 2 µm) at 50°C. Mobile phase A was 0.1% formic acid and mobile phase B was 80% acetonitrile, 0.1% formic acid. For the TMT peptides, the gradient method included: 150 min gradient 5%-38% B, 10 min up to 95% B, 5 min isocratic at 95% B, re-equilibration to 5% B in 5 min and 10 min isocratic at 5% B at flow rate 300 nL/min.

Survey scans were acquired in the range of 375-1,500 m/z with mass resolution of 120 k, AGC 4×10^5 and max injection time (IT) 50 ms. Precursors were selected with the top speed mode in cycles of 3 sec and isolated for HCD fragmentation with quadrupole isolation width 0.7 Th. Collision energy was 38% with AGC 1×10^5 and max IT 86 ms. Targeted precursors were dynamically excluded for further fragmentation for 45 seconds with 7 ppm mass tolerance.

Database search and protein quantification

The mass spectra were analysed in Proteome Discoverer 2.4 (Thermo Scientific) with the SequestHT search engine for protein identification and quantification. The precursor and fragment ion mass tolerances were set at 20 ppm and 0.02 Da respectively. Spectra were searched for fully tryptic peptides with maximum 2 missed-cleavages. TMT 6plex at N-terminus/K and Carbamidomethyl at C was selected as static modification and Oxidation of M and Deamidation of N/Q were selected as dynamic modifications.. Peptide confidence was estimated with the Percolator node and peptides were filtered at q-value<0.01 based on decoy database search. All spectra were searched against reviewed UniProt Homo Sapiens protein entries. The reporter ion quantifier node included a TMT 10plex quantification method with an integration window tolerance of 15 ppm. Only unique peptides were used for quantification, considering protein groups for peptide uniqueness. Only peptides with average reporter signal-to-noise>3 were used for protein quantification. Proteins were normalised based on total peptide signal-to-noise per sample and scaled to mean across samples (mean=100). Statistical analysis was performed in Perseus 1.6. Log2ratios of knock-downs versus matched controls were computed followed by column z-score transformation. Differentially expressed proteins were defined by one-sample t-test using the different clones as replicates. Proteins with log2 FC (z-scored) < -1 or > 1 with p-value < 0.05 were considered as differentially expressed.

RNA-sequencing data and gene expression analysis

Poly(A)+ selected reverse stranded RNA sequencing libraries were prepared from total RNA using KAPA mRNA HyperPrep Library kit for Illumina® kit, with 200 ng of total RNA as input. Libraries were sequenced on a HiSeq 4000 platform. A total of 30 million of 100 bp-long paired-end strand-specific reads were sequenced per sample. Raw mRNA sequencing reads were trimmed using TrimGalore (https://www.bioinformatics.babraham.ac.uk/projects/trim_galore), quality evaluated using FastQC 0.11.7, (https://www.bioinformatics.babraham.ac.uk/projects/fastqc/) and aligned to GRCh38.p13 human genome using splice-aware aligner STAR v2.6.1 [37] with default parameters. Aligned reads were quantified using --quantMode (TranscriptomeSAM GeneCounts) function. All samples had a percentage of uniquely map reads over 90%.

Differential gene expression was measured using DESeq2 [38] using STAR count matrix as an input (DESeqDataSetFromMatrix function*)*. Results were generated by comparing siRNA control to siRNA IMP1 transfected cells in neurons or NPC. A gene was considered significantly differentially expressed if p-value < 0.05 and log2 FC < -1.5 for downregulated genes and > 1.5 for upregulated genes. To remove background, genes with zero counts were excluded. For comparing gene expression level between NPC and neurons we reanalysed previously generated RNA-seq data from the lab [32] - GSE98290. Fastq files from controls samples at day 14 (NPC) and day 21 (neurons) of differentiation (SRR5483813, SRR5483814, SRR5483799, SRR5483815, SRR5483812, SRR5483797, SRR5483798) were aligned to GRCh38.p13 human genome using STAR v2.6.1. and using gencode.v36.annotation.gtf file (--sjdbGTFfile). Aligned reads were quantified using --quantMode (TranscriptomeSAM GeneCounts) function. Bedgraph files were generated using Deeptools' bamcoverage package [39] with default parameters

Processing of iCLIP data

iCLIP reads from 9 neurons and NPC samples and IgG control were processed according to iCLIP analysis methods using the iMaps webserver (https://imaps.genialis.com/iclip) for standardised primary analysis. iMaps is based on the icount package [40]. Briefly, the following steps were performed: demultiplexing using experimental barcodes, UMI identification, adapter trimming, STAR pre-mapping to rRNAs and tRNAs, STAR alignment to genome, crosslink site assignment, duplicate removal by UMI sequence, peak calling (paraclu), generation of summary files based on crosslink events on gene type, biotype, or gene region. Significant crosslink sites were defined using the 'iCount peaks' tool on the iMaps web server while peaks were defined by clustering the significant crosslink sites using default parameters. Control quality checks (FastQC 0.11.7, https://www.bioinformatics.babraham.ac.uk/projects/fastqc/, PCR duplication ratio, quality of sequencing and alignment statistics from iMaps) were performed on each individual sample. All samples showed a high quality with low PCR duplicate ratio (1.8 to 6.1). All samples had a similar number of uniquely mapped reads (on average 7. 3E+06 for neurons and 5.7E+06 for NPC) except for two NPC samples which were further excluded in the analysis. Crosslink or peak bed files from biological and technical replicates for neurons (9) and NPC (7) samples were merged using iMaps group function. Peaks were then called and the output bed or bedgraph files were used for further analysis. For all samples the human GRCh38 genome build and GENCODE version 36 annotation were used. For comparison between neurons and NPC sample and to account for gene expression, normalisation at gene level was performed using Deseq2 by inputting the number of IMP1 crosslink count per gene obtained from iMaps and using gene count values obtained from RNAseq experiment (GSE98290, see "RNA-sequencing data and gene expression analysis" section) as a covariate. When required normalisation for library size was performed within the DESeq2 analysis or *clipplotR* (see visualisation of iCLIP and miCLIP data method section). PCA plots were performed using the number of crosslink counts per gene obtained from iMaps.

miCLIP analysis and m6A site calling

miCLIP reads from 8 neurons and NPC samples and non-crosslinked control were processed according to iCLIP analysis methods using the iMaps web server for standardised primary analysis (See "Processing of iCLIP data"). Significant crosslink sites were defined using the 'iCount peaks' tool on the iMaps web server while peaks were defined by clustering the significant crosslink sites using default parameters. Control quality check

(FastQC report, PCR duplication ratio, quality of sequencing and alignment statistics) was performed on each individual sample. Two samples were discarded based on unique counts number and PCR duplicate ratios. The other samples showed a high quality with low PCR duplicate ratio (1.9 to 15). Correlation between replicates was assessed using DeepTools' multibamSummary function. Default parameters were used except for binSize (50,000 bases was used). Heatmap was then plotted with DeepTools' plotCorrelation function using Pearson method. Mutation (CIMS) and Truncation (CITS) site calling was performed as previously described [39]. Briefly, low-quality bases and adaptor sequences were all removed using FLEXBAR tool
(-f i1.8 -as AGATCGGAAGAGCGGTTCAG --pre-trim-phred 30 -s -t sample). Reads were demultiplexed based on 5′ barcodes for individual replicates using pyCRAC [41]. Reads were processed in pooled or separate replicate modes using the CTK package (https://zhanglab.c2b2.columbia.edu/index.php/CTK_Documentation).
In brief the barcode was stripped and added to the name of the read. Biological and technical replicates were concatenated (CIMS analysis). PCR duplicates were collapsed using pyFastqDuplicateRemover.py script from pyCRAC. The header was transformed to be compatible with CTK analysis (mawk -F '[_/]' '/^>/{print $1"_"$2"_"$3"/"$4"#"$3"#"$2; getline($9); print $9}'). Reads were aligned to the human genome (hg38) using bwa (aln -t 4 -n 0.06 -q 20). Positions of C → T from mapped reads were obtained using the CIMS software package [42]. Briefly, aligned reads were parsed using parseAlignment.pl to generate a bed file of read coordinates and mutation coordinates. PCR duplicates were collapsed based on read coordinated and barcode identities using tag2collapse.pl script. To get the mutations in unique tags joinWrapper.py script was used. C to T transitions were extracted and a bed file generated. Mutation reproducibility was evaluated using CIMS.pl script. For each mismatch position, the unique tag coverage (*k*) and the number of C→T transitions (*m*) were determined. C→T transitions located in DRACH motifs were called using kmer.annotate.cims.sh script based on (m ≥ 2 or m ≥ 5) and transition frequency (1% ≥ m/k ≤ 50%). Position of truncations from mapped reads were obtained using the CITS software package [43]. Briefly, after the mutation removal step from PCR duplicates in the CIMS strategy, deletions were obtained from the mutation file using getMutationType.pl on each individual sample. Truncations events were then identified using CITS.pl script. Files with $P<0.05$ or $P < 0.001$ were used for further analysis. Technical and biological replicates were then concatenated. CITS and CIMS final bed files were merged using Bedtools's mergeBed function.

Analysis of enrichment of IMP1 peaks and IMP1-m6A peaks

IMP1 and m6A bed files were annotated by interesting them using bedtools' mergeBed package[44] with gencode.v36.annotation.gtf file downloaded from https://www.gencodegenes.org/human/release_36.html and converted into bed file using BEDOPS[45](gtf2bed). Annotated IMP1 and m6A bed files were filtered for protein-coding genes and processed to produce a table of IMP1 or m6A counts per gene. To obtain the number of IMP1-m6A peaks per gene, an overlap between IMP1 and m6A bed files was performed using the bedtools' intersect package. The resulting bed file was filtered for protein-coding genes and was processed to produce a table of count per genes of m6A sites bound by IMP1. The protein expression data was obtained from the proteomics dataset. The

enrichment score was obtained from the Log2ratios of knockdowns versus matched controls followed by column z-score transformation. A pseudocount of 0.001 was added to the expression values to avoid division with 0. The cumulative distribution function was calculated for genes grouped by m6A count or IMP1 peaks and plotted using R (ecdf package).

Quantification of microtubules enrichment terms

Percentage of proteins belonging to the “microtubules-based process” term” was calculated as follow: PANTHER GO analysis was performed on downregulated proteins from the MS experiment, or downregulated proteins from MS experiment containing IMP1 peaks in the corresponding RNA as defined by iCLIP, or downregulated proteins from MS experiment with m6A-IMP1 peaks in the corresponding RNA as defined by iCLIP and miCLIP. The percentage of protein belonging to the term “microtubules-based process” was quantified based on the total number of proteins in each corresponding dataset.

Motif analysis

De novo motif enrichment was performed on peak bed files using HOMER’s (Hypergeometric Optimization of Motif EnRichment) findMotfisGenome.pl package using a search for RNA motifs with a length of 5 (-rna -len 5) and default settings for the other parameters (http://homer.ucsd.edu/homer/motif/rnaMotifs.html).

Gene Ontology

GO analysis was performed using protein analysis through evolutionary relationships (PANTHER) version 16.0 (http://geneontology.org) for the biological process category, with the organism set to Homo sapiens. Results were sorted hierarchically using the default parameters (test type: Fisher's Exact, correction: FDR). When mentioned in the legend, redundant GO terms were removed using REVIGO [46] (Reduce & Visualize Gene Ontology) allowing medium GO term similarity.

Protein-protein interaction network analysis

Interactions between proteins were investigated using the STRING database (Search Tool for the Retrieval of Interacting Genes/Proteins). Default parameters were used.

Visualisation of iCLIP and miCLIP data

CLIP data were visualised in a comparative manner on individual transcripts using the software *clipplotr* (https://github.com/ulelab/clipplotr). iCLIP signals were normalised on library size and scaled to crosslinks per million. Rolling means smoothing with a sliding window of 100 nucleotides was used. When specified in the legend Integrative Genomics Viewer (IGV) software was used.

Generation of nervous system m6A map

To generate a map of previously detected m6A sites in nervous tissue, bed files from published miCLIP and MeRIP-seq datasets were downloaded from Gene Expression Omnibus (GEO) repository - GSE106607, GSE106423, GSE71154, GSE29714, GSE37005 or obtained directly from publication (supplementary data) Yu et al. 2020 [48]. When necessary, genome coordinates were converted to hg38 genome assembly using Lift Genome Annotations (https://genome.ucsc.edu/cgi-bin/hgLiftOver). Duplicated reads were first removed.

When a dataset contained information from different conditions, it was split into corresponding bed files based on sample ID. Bed files related to the nervous system (brain and neurons) were then merged using the merge command line from Bedtools v2.30.0. with default parameters. Overlap between the nervous dataset and neuron miCLIP bed files was performed using bedtool's intersect package with default parameters.

Metagene plots

Metagene plots were generated from CITS and CIMS bed files using MetaPlotR pipeline as previously described [47].

Statistical analysis

Statistical analyses were performed using RStudio (v. 4.1.2), or GraphPad Prism 7. Normality was assessed using the D'Agostino-Pearson omnibus K2 normality test. For analyses where some, or all, datasets failed a normality test, a non-parametric analysis was considered. Paired or unpaired two-tailed Student's t-test was performed when comparing two categories, except where stated otherwise. When more than two groups were compared, one-way ANOVA was used, except where stated otherwise. For cumulative distribution, a two-sided Kolmogorov–Smirnov test was used to calculate P-values. P-values less than 0.05 were considered to be significant. Graphs and error bars reflect means +/- s.e.m., except where stated otherwise.

Data analysis

Data analyses were performed with Microsoft Excel, Graphpad Prism 7, ImageJ (v 2.3.0), RStudio (v 4.1.2) which were also used to generate graphs. Illustrations were created with BioRender.com.

Data availability

The RNA-seq, iCLIP and miCLIP data generated for this paper have been deposited in NCBI Gene Expression Omnibus (GEO) under accession number GSE203571. RNA-seq data used to estimate the mRNA expression level in NPC and neurons were obtained from GEO under accession number GSE98290. miCLIP and MeRIP-seq to generate nervous tissue m6A map were from GEO under accession number GSE106607, GSE106423, GSE71154, GSE29714, GSE37005 and dataset from Yu et al. 2020 [48]. The mass spectrometry raw data have been deposited to PRIDE accession number PXD034341. All other data are available from the corresponding author upon reasonable request.

Acknowledgements

Thanks are due to Jernej Ule and his team in particular Flora Lee, Rupert Faraway, Charlotte Capitanchik, Klara Kuret for crucial advice and discussion for the design of iCLIP and miCLIP experiments as well as the access to reagents and protocols. We would like to thank Yoh Isogai for useful discussions and help during the design of the project, and for critical reading of the manuscript. We would also like to thank Giancarlo Abis, and other members of the Ramos and Patani labs for experimental support, comments and suggestions on the project and manuscript; members of the Crick Advanced Sequencing and Light Microscopy Facilities and the Institute Cancer Research (ICR) proteomics core facility for support.

Author contribution

P.K., R.P. and A.R. conceived the project, J.H. performed and analysed immunofluorescence experiments, H.C and P.K. performed the miCLIP experiment, T.I.R. and J.S.C. performed mass spectrometry analysis, P.K. performed all other experiments, S.E.S., A.M.C., R.L and P.K. performed bioinformatics analysis, P.K., R.P. and A.R. wrote the manuscript with input from all authors.

Fundings

P.K. and A.R. are supported by the UK Medical Research Council research grant S000305/1. A.R. is also supported by the UK BBRSC research grant S014438/1. R.P. is supported by an MRC Senior Clinical Fellowship (MR/S006591/1) and a Lister Research Prize Fellowship. R.L. is supported by the Idiap Research Institute. This work was also supported by the Francis Crick Institute, which receives its core funding from Cancer Research UK (FC010110), the UK Medical Research Council (FC010110), and the Wellcome Trust (FC010110). The proteomics work of T.I.R. and J.S.C. was funded by the CRUK Centre grant with reference number C309/A25144. For the purpose of open access, the authors have applied a Creative Commons Attribution (CC BY) licence to any Author Accepted Manuscript version arising.

Competing interest contribution

The authors declare no competing interest.

1. Hansen, T. V. O. *et al.* Dwarfism and impaired gut development in insulin-like growth factor II mRNA-binding protein 1-deficient mice. *Mol. Cell. Biol.* **24**, 4448–4464 (2004).
2. Nishino, J., Kim, S., Zhu, Y., Zhu, H. & Morrison, S. J. A network of heterochronic genes including Imp1 regulates temporal changes in stem cell properties. *Elife* **2**, e00924 (2013).
3. Perycz, M., Urbanska, A. S., Krawczyk, P. S., Parobczak, K. & Jaworski, J. Zipcode binding protein 1 regulates the development of dendritic arbors in hippocampal neurons. *J. Neurosci.* **31**, 5271–5285 (2011).
4. Eom, T., Antar, L. N., Singer, R. H. & Bassell, G. J. Localization of a beta-actin messenger ribonucleoprotein complex with zipcode-binding protein modulates the density of dendritic filopodia and filopodial synapses. *J. Neurosci.* **23**, 10433–10444 (2003).
5. Fallini, C., Donlin-Asp, P. G., Rouanet, J. P., Bassell, G. J. & Rossoll, W. Deficiency of the Survival of Motor Neuron Protein Impairs mRNA Localization and Local Translation

in the Growth Cone of Motor Neurons. *J. Neurosci.* **36**, 3811–3820 (2016).

6. Hüttelmaier, S. *et al.* Spatial regulation of β-actin translation by Src-dependent phosphorylation of ZBP1. *Nature* vol. 438 512–515 (2005).
7. Zhang, H. L. *et al.* Neurotrophin-induced transport of a beta-actin mRNP complex increases beta-actin levels and stimulates growth cone motility. *Neuron* **31**, 261–275 (2001).
8. Stöhr, N. *et al.* ZBP1 regulates mRNA stability during cellular stress. *J. Cell Biol.* **175**, 527–534 (2006).
9. Huang, H. *et al.* Recognition of RNA N-methyladenosine by IGF2BP proteins enhances mRNA stability and translation. *Nat. Cell Biol.* **20**, 285–295 (2018).
10. Nielsen, J. *et al.* A family of insulin-like growth factor II mRNA-binding proteins represses translation in late development. *Mol. Cell. Biol.* **19**, 1262–1270 (1999).
11. Noubissi, F. K. *et al.* CRD-BP mediates stabilization of βTrCP1 and c-myc mRNA in response to β-catenin signalling. *Nature* vol. 441 898–901 (2006).
12. Farina, K. L., Hüttelmaier, S., Musunuru, K., Darnell, R. & Singer, R. H. Two ZBP1 KH domains facilitate β-actin mRNA localization, granule formation, and cytoskeletal attachment. *Journal of Cell Biology* vol. 160 77–87 (2003).
13. Ross, A. F., Oleynikov, Y., Kislauskis, E. H., Taneja, K. L. & Singer, R. H. Characterization of a beta-actin mRNA zipcode-binding protein. *Mol. Cell. Biol.* **17**, 2158–2165 (1997).
14. Yisraeli, J. K. VICKZ proteins: a multi-talented family of regulatory RNA-binding proteins. *Biol. Cell* **97**, 87–96 (2005).
15. Nielsen, F. C., Nielsen, J., Kristensen, M. A., Koch, G. & Christiansen, J. Cytoplasmic trafficking of IGF-II mRNA-binding protein by conserved KH domains. *Journal of Cell Science* vol. 115 2087–2097 (2002).
16. Noubissi, F. K. *et al.* CRD-BP mediates stabilization of βTrCP1 and c-myc mRNA in response to β-catenin signalling. *Nature* **441**, 898–901 (2006).
17. Conway, A. E. *et al.* Enhanced CLIP Uncovers IMP Protein-RNA Targets in Human

Pluripotent Stem Cells Important for Cell Adhesion and Survival. *Cell Rep.* **15**, 666–679 (2016).

18. Hüttelmaier, S. *et al.* Spatial regulation of beta-actin translation by Src-dependent phosphorylation of ZBP1. *Nature* **438**, 512–515 (2005).
19. Wu, B., Buxbaum, A. R., Katz, Z. B., Yoon, Y. J. & Singer, R. H. Quantifying Protein-mRNA Interactions in Single Live Cells. *Cell* **162**, 211–220 (2015).
20. Cruz-Zaragoza, L. D. *et al.* An in vitro system to silence mitochondrial gene expression. *Cell* **184**, 5824–5837.e15 (2021).
21. Yoon, K.-J. *et al.* Temporal Control of Mammalian Cortical Neurogenesis by m6A Methylation. *Cell* vol. 171 877–889.e17 (2017).
22. Meyer, K. D. *et al.* Comprehensive analysis of mRNA methylation reveals enrichment in 3' UTRs and near stop codons. *Cell* **149**, 1635–1646 (2012).
23. Chang, M. *et al.* Region-specific RNA mA methylation represents a new layer of control in the gene regulatory network in the mouse brain. *Open Biol.* **7**, (2017).
24. Dominissini, D. *et al.* Topology of the human and mouse m6A RNA methylomes revealed by m6A-seq. *Nature* **485**, 201–206 (2012).
25. Lence, T. *et al.* m6A modulates neuronal functions and sex determination in Drosophila. *Nature* vol. 540 242–247 (2016).
26. Geula, S. *et al.* Stem cells. m6A mRNA methylation facilitates resolution of naïve pluripotency toward differentiation. *Science* **347**, 1002–1006 (2015).
27. Poh, H. X., Mirza, A. H., Pickering, B. F. & Jaffrey, S. R. Understanding the source of METTL3-independent m6A in mRNA. doi:10.1101/2021.12.15.472866.
28. Menon, S. & Gupton, S. L. Building Blocks of Functioning Brain: Cytoskeletal Dynamics in Neuronal Development. *Int. Rev. Cell Mol. Biol.* **322**, 183–245 (2016).
29. Sakakibara, A., Ando, R., Sapir, T. & Tanaka, T. Microtubule dynamics in neuronal morphogenesis. *Open Biology* vol. 3 130061 (2013).
30. Fiock, K. L., Smalley, M. E., Crary, J. F., Pasca, A. M. & Hefti, M. M. Increased Tau Expression Correlates with Neuronal Maturation in the Developing Human Cerebral

Cortex. *eNeuro* **7**, (2020).

31. Hall, C. E. *et al.* Progressive Motor Neuron Pathology and the Role of Astrocytes in a Human Stem Cell Model of VCP-Related ALS. *Cell Reports* vol. 19 1739–1749 (2017).
32. Luisier, R. *et al.* Intron retention and nuclear loss of SFPQ are molecular hallmarks of ALS. *Nat. Commun.* **9**, 2010 (2018).
33. Carpenter, A. E. *et al.* CellProfiler: image analysis software for identifying and quantifying cell phenotypes. *Genome Biol.* **7**, R100 (2006).
34. Schindelin, J. *et al.* Fiji: an open-source platform for biological-image analysis. *Nat. Methods* **9**, 676–682 (2012).
35. Huppertz, I. *et al.* iCLIP: Protein–RNA interactions at nucleotide resolution. *Methods* vol. 65 274–287 (2014).
36. Hawley, B. R. & Jaffrey, S. R. Transcriptome-Wide Mapping of m6A and m6Am at Single-Nucleotide Resolution Using miCLIP. *Current Protocols in Molecular Biology* vol. 126 e88 (2019).
37. Dobin, A. *et al.* STAR: ultrafast universal RNA-seq aligner. *Bioinformatics* **29**, 15–21 (2013).
38. Love, M. I., Huber, W. & Anders, S. Moderated estimation of fold change and dispersion for RNA-seq data with DESeq2. *Genome Biol.* **15**, 550 (2014).
39. Ramírez, F. *et al.* deepTools2: a next generation web server for deep-sequencing data analysis. *Nucleic Acids Res.* **44**, W160–5 (2016).
40. König, J. *et al.* iCLIP reveals the function of hnRNP particles in splicing at individual nucleotide resolution. *Nat. Struct. Mol. Biol.* **17**, 909–915 (2010).
41. Webb, S., Hector, R. D., Kudla, G. & Granneman, S. PAR-CLIP data indicate that Nrd1-Nab3-dependent transcription termination regulates expression of hundreds of protein coding genes in yeast. *Genome Biol.* **15**, R8 (2014).
42. Zhang, C. & Darnell, R. B. Mapping in vivo protein-RNA interactions at single-nucleotide resolution from HITS-CLIP data. *Nat. Biotechnol.* **29**, 607–614 (2011).
43. Weyn-Vanhentenryck, S. M. *et al.* HITS-CLIP and integrative modeling define the Rbfox

splicing-regulatory network linked to brain development and autism. *Cell Rep.* **6**, 1139–1152 (2014).

44. Quinlan, A. R. & Hall, I. M. BEDTools: a flexible suite of utilities for comparing genomic features. *Bioinformatics* **26**, 841–842 (2010).
45. Neph, S. *et al.* BEDOPS: high-performance genomic feature operations. *Bioinformatics* **28**, 1919–1920 (2012).
46. Supek, F., Bošnjak, M., Škunca, N. & Šmuc, T. REVIGO summarizes and visualizes long lists of gene ontology terms. *PLoS One* **6**, e21800 (2011).
47. Olarerin-George, A. O. & Jaffrey, S. R. MetaPlotR: a Perl/R pipeline for plotting metagenes of nucleotide modifications and other transcriptomic sites. *Bioinformatics* **33**, 1563–1564 (2017).
48. Yu, J. *et al.* Epitranscriptomic profiling of N6-methyladenosine-related RNA methylation in rat cerebral cortex following traumatic brain injury. *Mol. Brain* **13**, 11 (2020).